

# Asynchronous Fractional Multi-Agent Deep Reinforcement Learning for Age-Minimal Mobile Edge Computing

Lyudong Jin, Ming Tang, *Member, IEEE*, Jiayu Pan, Meng Zhang, *Member, IEEE*, Hao Wang, *Member, IEEE*

**Abstract**—In the realm of emerging real-time networked applications such as cyber-physical systems (CPS), the *Age of Information* (AoI) has emerged as a pivotal metric for evaluating the timeliness. To meet the high computational demands, such as those in smart manufacturing within CPS, mobile edge computing (MEC) presents a promising solution for optimizing computing and reducing AoI. In this work, we study the timeliness of compute-intensive updates and explore jointly optimizing the task updating (when to generate a task) and offloading (where to process a task) policies to minimize AoI. Specifically, we consider edge load dynamics and formulate a task scheduling problem to minimize the expected time-average AoI. Solving this problem is challenging due to the fractional objective introduced by AoI and asynchronous decision-making of the semi-Markov game (SMG). To this end, we propose a fractional reinforcement learning (RL) framework. We begin by introducing a fractional single-agent RL framework and establish its linear convergence rate. Building on this, we develop a fractional multi-agent RL framework, extend Dinkelbach’s method, and demonstrate its equivalence to the inexact Newton’s method. Furthermore, we provide the conditions under which the framework achieves linear convergence to the Nash equilibrium (NE). To tackle the challenge of asynchronous decision-making in the SMG, we further design an asynchronous model-free fractional multi-agent RL algorithm, where each mobile device can determine the task updating and offloading decisions without knowing the real-time system dynamics and decisions of other devices. Experimental results show that when compared with the best existing baseline algorithm, our proposed algorithm reduces the average AoI by up to 50.6%.

**Index Terms**—Age of Information, mobile edge computing, Nash equilibrium, reinforcement learning, multi-agent reinforcement learning

## I. INTRODUCTION

### A. Background and Motivations

Real-time embedded systems and mobile devices, including smartphones, IoT devices, and wireless sensors, have rapidly proliferated. This growth is driven by cyber-physical systems

Lyudong Jin and Meng Zhang are with the Zhejiang University—University of Illinois at Urbana-Champaign Institute, Zhejiang University, Haining 314400, China (e-mail: 3180101183@zju.edu.cn; mengzhang@intl.zju.edu.cn).

Ming Tang is with the Department of Computer Science and Engineering, Southern University of Science and Technology, Shenzhen 518000, China (e-mail: tangm3@sustech.edu.cn).

Jiayu Pan is with the School of Software Technology, Zhejiang University, Ningbo 315048, China (e-mail: jiayupan26@zju.edu.cn).

Hao Wang is with the Department of Data Science and AI, Faculty of Information Technology, Monash University, Melbourne, Victoria 3800, Australia (e-mail: hao.wang2@monash.edu).

Part of this paper was presented in AAAI-24 [1].

(CPS) applications including collaborative autonomous driving for autonomous logistics (e.g., [2]), smart energy systems (e.g., [3]), and smart manufacturing (e.g., [4]). These applications generate a large amount of data and require intensive computational processing, which in turn creates a pressing need for low-latency, reliable, and private task execution. Mobile edge computing (MEC), also known as multi-access edge computing [5], addresses these needs by offloading computational tasks from end devices to nearby edge servers [6]. In this way, MEC reduces latency compared to cloud computing and provides larger computational capacity than that of mobile computing.

Timely information updates are crucial for the aforementioned emerging CPS applications with high computational demands. These updates depend on real-time sensory data and computational results, such as human interaction and safety data, environmental data, and positioning and motion data. For instance, critical applications (e.g., [7], [8]), such as collaborative robots in smart manufacturing that operate alongside humans, require split-second decision-making to ensure safety and efficiency, relying on computationally intensive tasks like object detection, path planning, and task execution [9]. However, local computing often struggles to meet these stringent timeliness requirements, potentially compromising system performance and safety. This need for data freshness has driven the development of a new metric, *Age of Information* (AoI) [10], which quantifies the time elapsed since the most recently delivered data or computational results were produced, providing an accurate measure of information timeliness.

While numerous prior studies on MEC have focused on minimizing delay (e.g., [11], [12]), they often overlooked AoI, which is crucial for real-time applications. Here we highlight the huge difference between delay and AoI. Specifically, task delay measures the duration between task generation and task output reception. With less frequent updates (i.e., when tasks are generated at a lower frequency), task delays are naturally smaller due to reduced queuing delays from empty queues. In contrast, AoI considers both task delay and the output freshness. To minimize AoI for compute-intensive tasks, the update frequency must be balanced to reduce individual task delays while ensuring the freshness of the most recent task output. This difference between delay and AoI reveals a counterintuitive phenomenon in age-minimal scheduling: mobile devices may need to wait before generating new tasks after receiving a task output. Specifically, a key bottleneck in CPS

is the requirement for timely operation. Although low-latency communication is necessary, research has shown that it alone cannot guarantee timely system performance (see [13], [14]).

Consequently, AoI has been proposed as a more suitable metric than latency for ensuring timely updates in CPS systems.

In this paper, we aim to answer the key question as follows.

**Key Question.** *How should mobile devices optimize their updating and offloading policies in real-time MEC systems in order to minimize AoI?*

### B. Challenges

Optimizing AoI in MEC systems with time-varying channels requires a sophisticated scheduling policy for mobile devices, involving two key decisions: updating and offloading. The *updating* decision determines the interval between task completion and the initiation of the next task generation, while the *offloading* decision decides whether to process the task locally or offload it to a specific edge server. Given the success of multi-agent reinforcement learning (MARL) in MEC systems [15], we aim to design a fractional MARL framework with theoretical analysis and propose an asynchronous fractional multi-agent deep reinforcement learning (MADRL) to optimize the task scheduling policy. Several significant challenges of our paper are presented as follows.

*How to deal with the fractional nature of AoI objective in RL?* Many prior works on MEC have explored offloading (e.g., [12], [16]–[19]), and some have considered AoI (e.g. [18]–[20]). However, they did not consider the fractional AoI objective. The fractional RL framework focuses on optimizing a fraction-of-expectation objective, making it challenging to directly evaluate the impact of actions on the objective, unlike the reward-based approach in the standard RL framework. Consequently, real-time MEC systems require a fractional RL framework to address the fractional AoI objective.

*How can we adapt the fractional framework to a multi-agent scenario?* Many MEC systems involve a decision-making process among multiple mobile devices. Effectively addressing this multi-agent paradigm in MARL is important for task scheduling in multi-agent systems. However, the fractional framework for a single agent cannot be directly adapted to the multi-agent scenario due to the increased complexity and inter-dependencies among agents. Thus, the MARL framework faces additional challenges in designing the fractional framework for the AoI objective.

*How to address the asynchronous decision problem in real-time MEC systems?* Traditional MADRL algorithms, such as multi-agent deep deterministic gradient descent (MADDPG) [21] assume that agents make decisions synchronously. However, in multi-agent MEC systems, each agent (mobile device) has different task update and processing durations, leading to asynchronous decision-making among agents. Traditional MADRL algorithms including QMIX [22] and MAPPO [23] would be inefficient to address the challenge of asynchronous control in MEC scheduling problem. Thus, addressing these challenges necessitates novel approaches that can effectively

handle the asynchronous nature of agent interactions in MEC environments.

### C. Solution Approaches and Contributions

In this paper, we propose a comprehensive framework that addresses the challenges of AoI optimization in MEC systems through both single-agent and multi-agent fractional reinforcement learning approaches for joint task updating and offloading policy optimization. We model the multi-agent interaction as a semi-Markov game (SMG), where agents' state transitions and rewards depend on asynchronous actions. Our solution framework consists of three key components. First, we propose a fractional RL framework based on Dinkelbach's fractional programming [24] for single-agent scenario. We then design a fractional MARL framework that incorporates Nash Q-learning [25] with fractional programming and inexact Newton method for the multi-agent scenario. Finally, to address the asynchronous decision-making nature of SMG, we develop an asynchronous fractional MARL framework with a novel asynchronous trajectory collection mechanism.

Our main contributions are summarized as follows:

- *Joint Task Updating and Offloading Problem:* We formulate a joint task updating and offloading problem, accounting for the fractional nature of AoI, the multi-agent system and the asynchronous decision-making processes of mobile devices. *To the best of our knowledge, this is the first work designing multi-agent asynchronous policies for the joint updating and offloading optimization in age-minimal MEC.*
- *Fractional RL Framework:* We consider the scenario of single-agent task scheduling and propose a fractional RL framework that integrates RL with Dinkelbach's method. This methodology can adeptly handle fractional objectives within the RL paradigm and demonstrates a linear convergence rate.
- *Fractional MARL Framework:* To tackle the challenge of fractional objectives in a multi-agent scenario, we begin by considering a Markov game, where state transitions and rewards depend on the agents' joint actions. We propose a novel fractional MARL framework that ensures the existence of a Nash equilibrium (NE) within this setting. Additionally, we extend Dinkelbach's method, demonstrating its equivalence to the inexact Newton's method, and provide the conditions under which it achieves linear convergence to the NE.
- *Asynchronous Fractional MADRL Algorithm:* We then propose a novel asynchronous fractional MADRL framework, built upon the centralized training with decentralized execution (CTDE) paradigm, to minimize AoI and approximate the NE in the SMG. Our framework integrates several key components as follows. First, we incorporate the dueling double deep Q-network (D3QN) and proximal policy optimization (PPO) into our fractional framework to handle hybrid action spaces. To address the asynchronous nature of SMGs, we implement a novel asynchronous trajectory collection mechanism. We also incorporate a recurrent neural network (RNN)

to synthesize information and evaluate other agents' strategies. These enhancements enable our framework to approximate the NE in the asynchronous environment of SMG and effectively minimize AoI for MEC systems.

- *Performance Evaluation:* Our experimental evaluation demonstrates that the asynchronous fractional MADRL algorithm outperforms benchmarks. When compared with the best existing baseline, our proposed algorithm improves the average AoI by up to 50.6%. The experimental results validate that both the fractional framework and the asynchronous mechanism contribute to enhancing the overall system performance.

## II. LITERATURE REVIEW

**Mobile Edge Computing:** Existing MEC research has explored various areas, including resource allocation [26], service placement [27], proactive caching [28], and task offloading [29]. Many studies have proposed RL-based approaches to optimize task delays in a centralized manner (e.g., [30], [31]) or in a decentralized manner (e.g., [12], [32]). *Despite the success in reducing the task delay, these approaches are NOT easily applicable to age-minimal MEC due to the challenges of fractional objective and asynchronous decision-making.*

**Multi-Agent RL in MEC:** Multi-Agent RL has been widely adopted in multi-agent approaches with decentralized manners in MEC systems. Li *et al.* proposed a decentralized edge server grouping algorithm and achieved NE by proving it to be exact potential game [33]. Chen *et al.* addressed the task offloading in the information freshness-aware air-ground integrated multi-access edge computing by letting each non-cooperative mobile user behave independently with local conjectures utilizing double deep Q-network. Feng *et al.* utilized a gating threshold to intelligently choose between local and global observations and limit the information transmission for approximating Nash equilibrium in an anti-jamming Markov game [34]. However, these MARL approaches have not considered the fractional objective when reaching NE.

**Age of Information:** Since its introduction by Kaul *et al.* [10], AoI has attracted increasing attention in the study of CPS (e.g., [35], [36]) in recent years. However, the majority of works have focused on the optimization of AoI in queueing systems and wireless networks, assuming the availability of complete and known statistical information (see [37], [38]).

Additionally, recent works have characterized the optimal sampling policies in single-source MEC systems [39] and further extended the analysis to joint sampling and scheduling optimization in multi-source systems [40]. However, the above studies analyzed either single-device or single-server scenarios and are difficult to adapt to the complex, time-varying dynamics of multi-user MEC systems where channel states and edge loads fluctuate unpredictably. A few studies have investigated RL algorithms design to minimize AoI in various application scenarios, including wireless networks [41], Internet-of-Things [42], autonomous driving [20], vehicular networks [43], and UAV-aided networks [44]. They mainly focused on optimizing resource allocation and trajectory design. Some works considered AoI as the performance metric for task offloading

in MEC and proposed RL-based approaches. For instance, Chen *et al.* in [19] considered AoI to capture the freshness of computation outcomes and proposed a multi-agent RL algorithm. *However, these works focused solely on designing task offloading policies without jointly optimizing updating policies. Note that none of these approaches have considered fractional RL and are difficult to directly address the problem in this paper.*

**RL with Fractional Objectives:** There is limited research on RL with fractional objectives. Ren *et al.* introduced fractional MDP [45]. Tanaka *et al.* [46] further studied partially observed MDPs with fractional costs. However, these studies have not extended to RL framework. Suttle *et al.* [47] proposed a two-timescale RL algorithm for fractional cost optimization. However, this method requires fixed reference states in Q-learning updates, which cannot be directly adapted to an asynchronous multi-agent environment.

**Asynchronous Decision-Making MARL:** Research on asynchronous decision-making in MARL is also limited. Xiao *et al.* [48] established an independent actor with individual centralized critic framework collecting historical information of each agent. But their approach disregards historical information from other agents and demands frequent policy updates via on-policy training. Chen *et al.* [49] proposed VarLenMARL in which each agent have a variable time step to gather the padding data of the most up-to-date step of other agents. However, this approach becomes inefficient with a large number of agents and may neglect information from agents that make decisions frequently. Wang and Sun [50] proposed a credit assignment framework with graph-based event critic for bus route control. However, this method only considers the effect of nearest upstream and downstream events of a single line and is not suitable for more complicated patterns including the effects from events of multiple lines. MAC-IAICC [48] formulates asynchronous actions as macro-actions and rigorously models the task within the MacDec-POMDP framework. Liang *et al.* addressed these issues with ASM-PPO [51] and ASM-HPPO [52], which collected agent trajectories independently and trained using available agents at each time slot. However, these methods could still suffer from the disruption of the synchronization of agents' tasks, as we will study later.

## III. SYSTEM MODEL

In this section, we present the system model for MEC. We first introduce the device and edge server model. We then define the AoI in our MEC setting and formulate the task scheduling problem within a semi-Markov game framework.

In this MEC system model, we consider mobile devices  $\mathcal{M} = \{1, 2, \dots, M\}$  and edge servers  $\mathcal{N} = \{1, 2, \dots, N\}$  respectively, as shown in Fig. 1. We denote the set of tasks as  $\mathcal{K} = \{1, \dots, K\}$ .

### A. Device Model

As shown in Fig. 1, each mobile device  $m$  is associated with a mobile user of CPS applications (e.g., [2]–[9]), who seeks to offload their computationally intensive tasks to edge

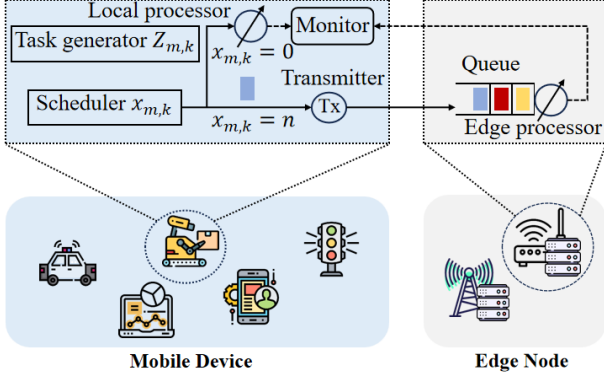


Fig. 1. An illustration of an MEC system with a mobile device  $m \in \mathcal{M}$  and an edge server  $n \in \mathcal{N}$  where the tasks offloaded by different mobile devices are represented using different colors.

servers to receive timely updates. Each mobile device includes a task generator, a scheduler, a monitor, and a local processor. The generator produces computational tasks. The scheduler chooses to process them locally or offload to an edge server. After the edge server or local processor processes the task, the result is sent to the monitor and the generator then decides when to initiate a new task.

**Generator:** We adopt a *generate-at-will* model, as considered in [53]–[57], where each mobile device’s task generator decides when to generate a new task. For example, tasks are generated alongside sensory data, with sensors specifically designed to sample physical phenomena on demand.<sup>1</sup> Specifically, when task  $k-1$  of mobile device  $m \in \mathcal{M}$  is completed at  $t'_{m,k-1}$ , the task generator observes the latency  $Y_{m,k-1}$  of task  $k-1$  and queue information of edge servers  $\mathbf{q}(t'_{m,k-1})$ .

The generator then decides on  $Z_{m,k} \geq 0$ , i.e., the waiting time before generating the *next* task  $k$ . We assume that edge servers share their load levels in response to mobile device queries. Since a generator produces a new task after the previous task is finished, the queue length is less than or equal to  $M$ , which incurs minimal signaling overhead. Let  $a_{m,k}^U$  denote the updating action for task  $k$ , i.e.,  $a_{m,k}^U = Z_{m,k}$  and  $\mathcal{A}^U = \mathbb{R}_+^M$  be the updating action space, where  $\mathbb{R}_+$  denotes the space of non-zero real number. The generation time of task  $k$  is calculated as  $t_{m,k} = t'_{m,k-1} + Z_{m,k}$ . Notably, an optimal waiting strategy for updating can outperform a zero-wait policy, indicating that the waiting time  $Z_{m,k}$  is not necessarily zero and should be optimized for efficiency [53]. Specifically, our framework optimizes  $Z_{m,k}$  to find the optimal balance between the waiting time  $Z_{m,k}$  and potential queuing delays at the server, which is crucial in multi-agent environments where server availability is stochastic and transient.

**Scheduler:** When the generator produces task  $k$  at time  $t_{m,k}$ , the scheduler makes the offloading decision  $x_{m,k} \in$

$\{0\} \cup \mathcal{N}$  with the queue information  $\mathbf{q}(t_{m,k})$  of edge servers<sup>2</sup>. Let  $a_{m,k}^O$  denote the action of task  $k$  from mobile device  $m$ . That is,  $a_{m,k}^O = x_{m,k}$ ,  $k \in \mathcal{K}$ ,  $m \in \mathcal{M}$ . Let  $\mathcal{A}^O \in \{0\} \cup \mathcal{N}^M$  and  $\pi_m^O$  denote the offloading action space and the task offloading policy of mobile device  $m \in \mathcal{M}$ , respectively. For local processing on mobile device  $m \in \mathcal{M}$ ,  $\tau_{m,k}^{\text{local}}$  (in seconds) represents the processing time of task  $k$ . The value of  $\tau_{m,k}^{\text{local}}$  depends on the task size and the real-time computational capacity of mobile device (e.g., whether the device is busy in processing tasks of other applications). For offloading task  $k$  to edge server  $n \in \mathcal{N}$ ,  $\tau_{n,m,k}^{\text{tran}}$  (in seconds) denotes the transmission latency of mobile device  $m$ . The value of  $\tau_{n,m,k}^{\text{tran}}$  depends on the time-varying wireless channels. We assume that  $\tau_{m,k}^{\text{local}}$  is a random variable that follows exponential distributions, as in [32], [58], [59], to capture the inherent variability caused by stochastic computational complexity and resource contention in practical MEC environments.

### B. Edge Server Model

When a mobile device  $m \in \mathcal{M}$  offloads a task to edge server  $n \in \mathcal{N}$ , we consider the time-varying channels between mobile devices and edge nodes located at different positions. Considering Rayleigh fading, the instantaneous channel power gain between mobile user  $m$  and the edge server  $n$  at global time  $t$  is given by  $h_{t,m,n} = g_{t,m,n} d_{t,m,n}^{-\alpha}$ , where  $d_{t,m,n}$  is the distance from mobile user  $m$  to the edge node  $n$ , and  $\alpha$  is the path loss exponent, and  $g_{t,m,n}$  is the Rayleigh fading coefficient. Simultaneous transmissions from multiple devices to the same edge node can cause interference. According to the Shannon principle, the channel capacity for mobile device  $m$  with  $N$  orthogonal sub-channels of edge nodes, can be derived as:

$$R_{t,m,n} = W \log_2 \left( 1 + \frac{P_m h_{t,m,n}}{\eta_0 + \sum_{i \in \mathcal{N} \setminus \{m\}: c_i = c_m} \beta_{t,i} P_i h_{t,i,n}} \right), \quad (1)$$

where  $W$  is the channel bandwidth,  $P_m$  denotes the transmit power of mobile user  $m$ , and  $\eta_0$  represents the background noise power. The variable  $\beta_{t,i} \in \{0, 1\}$  indicates the transmission status of user  $i$  at time  $t$  ( $\beta_{t,i} = 1$  for active transmission and 0 otherwise). Note that the interference term implies that only mobile devices transmitting concurrently on the same sub-channel  $c_m$  contribute to the interference. Then, the transmitting time can be calculated as  $\tau_{n,m,k}^{\text{tran}} = l^k d^k / R_{t,m,n}$ .

When the mobile device  $m$  successfully offloads the task to edge server  $n$ , the task is stored in a queue waiting for processing, as shown in Fig. 1. We assume the queue operates on a first-come-first-served (FCFS) basis [37]. FCFS prevents strategic preemption to ensure game stability, while our generate-at-will setting inherently eliminates self-blocking. We denote  $\mathbf{q}(t) = \{q_n(t)\}_{n \in \mathcal{N}}$  as the queue lengths of all edge servers. Edge servers update their queue length information

<sup>1</sup>For the alternative model to the generate-at-will paradigm, where tasks arrive randomly, extending the proposed fractional RL framework is conceptually straightforward, as this can be achieved by simply removing the waiting action.

<sup>2</sup>Under the system model in Section III, observing the queue lengths of edge servers is sufficient for mobile devices to learn their offloading policies. Under a more complicated system (e.g., with device mobility), additional state information may be necessary. However, our proposed RL-based framework remain applicable with an extended state vector.

$q(t)$  in two cases: when a task is completed or when a waiting period ends. Recall that a generator generates a new task only after the previous task has been processed, the queue length is less than or equal to  $M$ . Thus, the information to be sent can be encoded in  $O(\log_2 M)$  bits with minimal signaling overheads. We denote  $w_{n,m,k}^{\text{edge}}$  (in seconds) as the duration that task  $k$  of mobile device  $m \in \mathcal{M}$  waits at the queue of edge server  $n$ . Let  $\tau_{n,m,k}^{\text{edge}}$  (in seconds) denote the latency of edge server  $n$  for processing task  $k$  of mobile device  $m$ . We assume that  $\tau_{n,m,k}^{\text{edge}}$  is a random variable following an exponential distribution i.e.,  $\tau_{n,m,k}^{\text{edge}} \sim \text{Exp}(\frac{C_n^{\text{edge}}}{l^k d^k})$ . Here,  $C_n^{\text{edge}}$  is the processing capacity (in GHz) of edge  $n$ . Parameters  $l^k$  and  $d^k$  denote the task size and task density of  $k$  respectively. In addition, the value of  $w_{n,m,k}^{\text{edge}}$  depends on the processing times of the tasks ahead in the queue, which are possibly offloaded by other mobile devices. Additionally, these offloading information cannot be directly observed by mobile device  $m$ . Therefore, the waiting time cannot be modeled analytically, motivating our use of a model-free MARL frameworks to capture such dynamics.

### C. Age of Information

For mobile device  $m$ , the AoI at global clock  $T$  [37] is defined by

$$\Delta_m(t) = t - T_m(t), \quad \forall m \in \mathcal{M}, t \geq 0, \quad (2)$$

where  $T_m(t) \triangleq \max_{k \in \mathcal{N}}(t_{m,k} | t'_{m,k} \leq t)$  stands for the time stamp of the most recently completed task.

The overall duration to complete task  $k$  is denoted by  $Y_{m,k} \triangleq t'_{m,k} - t_{m,k}$ . Therefore,

$$Y_{m,k} = \begin{cases} \tau_{m,k}^{\text{local}}, & x_{m,k} = 0, \\ \tau_{n,m,k}^{\text{tran}} + w_{n,m,k}^{\text{edge}} + \tau_{n,m,k}^{\text{edge}}, & x_{m,k} = n \in \mathcal{N}. \end{cases} \quad (3)$$

We consider a deadline  $\bar{Y}$  (in seconds). Tasks not completed within  $\bar{Y}$  seconds will be dropped [12], [60]. Meanwhile, the AoI keeps increasing until the next task is completed.

We define the trapezoid area associated with time interval  $[t_{m,k}, t_{m,k+1}]$ :

$$A(Y_{m,k}, Z_{m,k+1}, Y_{m,k+1}) \triangleq \frac{1}{2}(Y_{m,k} + Z_{m,k+1} + Y_{m,k+1})^2 - \frac{1}{2}(Y_{m,k+1})^2, \quad (4)$$

where  $Z_{m,k+1}$  denotes the updating interval before generating next task  $k+1$ . The time-average AoI is defined as  $\lim_{T \rightarrow \infty} \frac{1}{T} \int_0^T \Delta_m(t) dt$ . By applying the Renewal Reward Theorem, this time-average equals the ratio of the expected area per cycle (given by (4)) to the expected cycle duration. Thus, the objective for mobile device  $m$  is characterized as:

$$\Delta_m^{(\text{ave})} \triangleq \liminf_{K \rightarrow \infty} \frac{\sum_{k=0}^K \mathbb{E}[A(Y_{m,k}, Z_{m,k+1}, Y_{m,k+1})]}{\sum_{k=0}^K \mathbb{E}[Y_{m,k} + Z_{m,k+1}]}, \quad (5)$$

where  $\mathbb{E}[\cdot]$  is the expectation with respect to decisions made according to certain policies, which will be elaborated upon in the subsequent sections.

### D. Game Formulation

In MEC systems, mobile devices make updating and offloading decisions asynchronously due to variable transition times. These transition times fluctuate based on scheduling strategies and edge workloads. Given that the current MARL framework is designed for synchronous decision-making processes, it is not suitable for application in this context. To address this challenge, we model the real-time MEC scheduling problem as an SMG. An SMG extends Markov decision processes to multi-agent systems with variable state transition times. Thus, this framework can address asynchronous decision-making in MEC systems.

The game is defined as  $(\mathcal{M}, \mathcal{S}, \mathcal{A}, P_S, P_F, \mu_0)$ , given by

- $\mathcal{M}$ : the set of mobile devices;
- $\mathcal{S}$ : the state space denoted by  $\mathbb{N}^M \times \mathbb{N}^{NM} \times \mathbb{R}^M$ . Specifically, a state  $s \in \mathcal{S}$  is expressed as  $s \triangleq ((I_m)_{m \in \mathcal{M}}, (q(t_m))_{m \in \mathcal{M}}, (Y_m)_{m \in \mathcal{M}})$ , where  $(I_m)_{m \in \mathcal{M}}$  denotes the decision indicators, specifying whether each mobile device  $m \in \mathcal{M}$  needs to take offloading action  $a_m^0$ , updating action  $a_m^U$  or make no decisions;
- $\mathcal{A}$ : the action space defined as  $\mathcal{A}^U \times \mathcal{A}^O$ . Specifically, an action  $a \in \mathcal{A}$  consists of its task updating action  $a^U$  and task offloading action  $a^O$ . We define the set of admissible triplets as  $\mathcal{H} = \{(s, a) | s \in \mathcal{S}, a \in \mathcal{A}\}$ .
- $P_S : \mathcal{H} \rightarrow \mathbb{P}(\mathcal{S})$  is the transition function of the game, where  $\mathbb{P}(\mathcal{S})$  is the collection of probability distributions over space  $\mathcal{S}$ .
- $P_F : \mathcal{H} \times \mathcal{S} \rightarrow \mathbb{P}(\mathbb{R}^+)$ : the stochastic kernel determining the transition time distribution;
- $\mu_0$ : the distribution of the initial state  $s_0$ .

The key difference between a SMG and a conventional Markov game lies in the timing of state transitions. In a traditional Markov game, state transitions occur at fixed, discrete intervals, with agents acting synchronously at each step. In contrast, a SMG features asynchronous transitions, where the time between states is a non-negative random variable drawn from a distribution dependent on the current state and actions. Thus, the decision-making of each agent is asynchronous, with each agent acting independently based on its own timeline.

We define policy is denoted by  $\pi = \{\pi_m\}_{m \in \mathcal{M}}$ , where each policy  $\pi_m = (\pi_m^U, \pi_m^O)$  includes both the updating and offloading policies of single mobile device  $m$ . We define the expected long-term discounted AoI of mobile device  $m$  as

$$\mathbb{E}_\pi[\Delta_m] \triangleq \mathbb{E}_{s_0 \sim \mu_0} \left\{ \frac{\sum_{k=0}^{\infty} \delta^k \mathbb{E}_\pi[A(Y_{m,k}, Z_{m,k+1}, Y_{m,k+1})]}{\sum_{k=0}^{\infty} \delta^k \mathbb{E}_\pi[Y_{m,k} + Z_{m,k+1}]} \right\}, \quad (6)$$

where  $\delta \in (0, 1)$  is a discount factor. We have the objective with the initial state  $s_0$  under initial distribution  $\mu_0$ . For simplicity, we drop the notation  $\mathbb{E}_{s_0 \sim \mu_0}[\cdot]$ , which is by default unless stated otherwise in the following.

While standard RL is typically designed to maximize or minimize expected discounted cumulative rewards, the fractional RL framework focuses on optimizing a fraction-of-expectation objective function, as in (6). This means that it

is challenging to directly evaluate the impact of a specific action on the objective value, as is done with rewards in the conventional RL setting. This challenge primarily motivates our fractional RL framework, which also necessitates new analyses for convergence and algorithm design.

Note that the discounted AoI form facilitates the application of AoI optimization in RL and MARL frameworks that utilize discounted cost functions. By assigning less weight to costs incurred in the distant future, the objective in (6) encourages the agent to prioritize immediate information freshness in non-stationary environments, where long-term planning faces high uncertainty. Additionally, as  $\delta$  approaches 1, the discounted AoI (6) approximates the undiscounted AoI function (5). The expectation  $\mathbb{E}_\pi[\cdot]$  is taken with respect to the policy  $\pi$  and the time-varying system parameters, e.g., channels states, processing times and the edge loads. We define the Nash equilibrium  $\pi^* = \{\pi_m^*\}_{m \in \mathcal{M}}$  for our task scheduling problem as follows.

**Definition 1** (Nash Equilibrium). *In stochastic game  $\mathbf{G}$ , a Nash equilibrium is a tuple of policies  $(\pi_1^*, \dots, \pi_m^*)$  of cost functions such that for all  $m \in \mathcal{M}$  we have,*

$$\mathbb{E}_{\pi_m^*, \pi_{-m}^*}[\Delta_m] \leq \mathbb{E}_{\pi_m, \pi_{-m}^*}[\Delta_m]. \quad (7)$$

For each mobile device  $m \in \mathcal{M}$ , given the fixed stationary policies  $\pi_{-m}^*$ , the best response in our real-time MEC scheduling problem is defined as

$$\pi_m^* = \arg \underset{\pi_m}{\text{minimize}} \mathbb{E}_{\pi_m, \pi_{-m}^*}[\Delta_m]. \quad (8)$$

Solving (8) is challenging due to the following reasons. First, the fractional objective introduces a major challenge in obtaining the optimal policy for conventional RL algorithms due to its non-linear nature. Second, the multi-agent environment introduces complex dynamics from interactions between edge servers and mobile devices. Third, the continuous time nature, stochastic state transitions, and asynchronous decision-making in the SMG pose significant challenges in directly applying conventional game-theoretic methodologies.

In the following sections, we first analyze a simplified version of the single-agent fractional RL framework. This framework establishes a robust theoretical foundation and serves as a benchmark for subsequent experiments. We then extend our theoretical analysis of our fractional framework to multi-agent scenarios, which is closer to SMG and practical dynamics. Finally, we propose the fractional MADRL algorithm in asynchronous setting for SMG, which matches the practical dynamics of real-time MEC systems.

#### IV. FRACTIONAL SINGLE-AGENT RL FRAMEWORK

For foundational theoretical analysis, we first consider a fractional single-agent RL framework. We design a fractional MDP and propose a fractional Q-learning algorithm. We provide analysis of the linear convergence for this algorithm. We formulate the problem as follows.

##### A. Single-Agent Problem Formulation

Recall that agent  $m$  selects its updating action and scheduling action, satisfying  $(a_{m,k}^O, a_{m,k}^U) \in \mathcal{A}_m \triangleq \mathbb{R}^+ \times (\{0\} \cup \mathcal{N})$ . The goal of single-agent RL is to learn a stationary policy  $\pi_m$  that maps the state space  $\mathcal{S}$  to agent  $m$ 's action space  $\mathcal{A}_m$  via solving the following single-agent problem:

$$\pi_m^* = \arg \underset{\pi_m}{\text{minimize}} \mathbb{E}_{\pi_m}[\Delta_m], \quad (9)$$

where we focus on the policy of agent  $m$  alone, compared with (8).

We study the general fractional MDP framework and drop the index  $m$  in the rest of this section. We then introduce a fractional RL framework to address Problem (9). Specifically, we first reformulate Problem (9). We then introduce a fractional RL framework and propose a fractional Q-learning algorithm with provable convergence guarantees.

##### B. Dinkelbach's Reformulation

To solve Problem (9), we consider the Dinkelbach's reformulation. Specifically, we define a reformulated AoI in a discounted fashion:

$$\mathbb{E}_\pi[\Delta', \gamma] \triangleq \sum_{k=0}^{\infty} \delta^k \mathbb{E}_\pi[A(Y_k, Z_{k+1}, Y_{k+1}) - \gamma(Y_k + Z_{k+1})], \forall \gamma \geq 0. \quad (10)$$

Let  $\gamma^*$  be the optimal value of Problem (9). By leveraging Dinkelbach's method [24], we reformulate the problem as follows.

**Lemma 1** (Asymptotic Equivalence [24]). *Problem (9) is equivalent to the following reformulated problem:*

$$\pi^* = \arg \underset{\pi}{\text{minimize}} \mathbb{E}_\pi[\Delta', \gamma^*], \quad (11)$$

where  $\pi^*$  is the optimal solution to Problem (9).

Since  $\mathbb{E}_\pi[\Delta', \gamma^*] \geq 0$  for any  $\pi$  and  $\mathbb{E}_{\pi^*}[\Delta', \gamma^*] = 0$ ,  $\pi^*$  is also optimal for the Dinkelbach reformulation. This implies that the reformulation equivalence is also established for our stationary policy space.

##### C. Fractional MDP

We then extend the standard MDP to a fractional form, laying the groundwork for a more complex and practical setting in a Markov game.

A fractional MDP is defined as  $(\mathcal{S}, \mathcal{A}, P, c_N, c_D, Pr, \delta, \mu_0)$ , where  $\mathcal{S}$  and  $\mathcal{A}$  are the finite sets of states and actions, respectively;  $Pr$  is the state transition distribution;  $c_N$  and  $c_D$  are the fractional costs,  $\delta$  is a discount factor, and  $\mu_0 = \{\mu_0(s)\}_{s \in \mathcal{S}}$  denotes the initial global state distribution. We use  $\mathcal{Z}$  to denote the joint state-action space, i.e.,  $\mathcal{Z} \triangleq \mathcal{S} \times \mathcal{A}$ . We define the instant fractional costs at task  $k$  as

$$c_N(s_k, a_k) = A(Y_k, Z_{k+1}, Y_{k+1}), \quad (12)$$

$$c_D(s_k, a_k) = Y_k + Z_{k+1}. \quad (13)$$

---

**Algorithm 1** Fractional Q-Learning (FQL)

---

```

1: for episode  $i = 0, 1, \dots, E$  do
2:   Initialize  $s_0$ ;
3:   for task  $k = 0, 1, \dots, K$  do
4:     Observe the next state  $s_m(t+1)$ ;
5:     Observe a set of costs  $\{c_{N,k}, c_{D,k}\}$ ;
6:     Submit  $(s_k, a_k, c_{N,k}, c_{D,k}, s_{k+1})$ ;
7:   end for
8:    $\gamma_{i+1} = \frac{N_{\gamma_i}(s, a_i)}{D_{\gamma_i}(s, a_i)}$ , where  $a_i = \arg \min_a Q_{\gamma_i}(s, a)$ .
9: end for

```

---

From Lemma 1, Problem (9) has the equivalent Dinkelbach's reformulation:

$$\pi^* = \arg \min_{\pi} \lim_{K \rightarrow \infty} \mathbb{E}_{\pi} \left[ \sum_{k=0}^K \delta^k (c_N - \gamma^* c_D) \right], \quad (14)$$

where we can see from Lemma 1 that  $\gamma^*$  satisfies

$$\gamma^* = \min_{\pi} \lim_{K \rightarrow \infty} \frac{\mathbb{E}_{\pi} \left[ \sum_{k=0}^K \delta^k c_N \right]}{\mathbb{E}_{\pi} \left[ \sum_{k=0}^K \delta^k c_D \right]}. \quad (15)$$

Note that Problem (14) is a classical MDP problem, including an immediate cost  $c_N(s, a) - \gamma^* c_D(s, a)$ . Thus, we can apply a traditional RL algorithm to solve such a reformulated problem, such as Q-Learning or its variants (e.g., SQL in [61]).

However, the optimal quotient coefficient  $\gamma^*$  and the transition distribution  $P$  are not known *a priori*. Therefore, we design an algorithm that combines fractional programming and reinforcement learning to solve Problem (14) for a given  $\gamma$  and seek the value of  $\gamma^*$ . To achieve this, we start by introducing the following definitions.

Given a quotient coefficient  $\gamma$ , the optimal Q-function is

$$Q_{\gamma}^*(s, a) \triangleq \min_{\pi} Q_{\gamma}^{\pi}(s, a), \quad \forall (s, a) \in \mathcal{Z}, \quad (16)$$

where  $Q_{\gamma}^{\pi}(s, a)$  is the action-state function that satisfies the following Bellman's equation: for all  $(s, a) \in \mathcal{Z}$ ,

$$Q_{\gamma}^{\pi}(s, a) \triangleq c_N(s, a) - \gamma c_D(s, a) + \delta \mathbb{E}_{P_r} [Q_{\gamma}^{\pi}(s', a)], \quad (17)$$

where  $\mathbb{E}_{P_r}$  is a concise notation for  $\mathbb{E}_{s' \sim P_r(\cdot|s, a)}$ . In addition, we can further decompose the optimal Q-function in (16) into the following two parts:  $Q_{\gamma}^*(s, a) = N_{\gamma}(s, a) - \gamma D_{\gamma}(s, a)$  and, for all  $(s, a) \in \mathcal{Z}$ ,

$$N_{\gamma}(s, a) = c_N(s, a) + \delta \mathbb{E}_{P_r} [N_{\gamma}(s', a)], \quad (18)$$

$$D_{\gamma}(s, a) = c_D(s, a) + \delta \mathbb{E}_{P_r} [D_{\gamma}(s', a)]. \quad (19)$$

#### D. Fractional Q-Learning Algorithm

In this subsection, we present a Fractional Q-Learning (FQL) algorithm (see Algorithm 1). The algorithm consists of an inner loop with  $E$  episodes and an outer loop. The key

idea is to approximate the Q-function  $Q_{\gamma}^*$  using  $Q_i$  in the inner loop, while iterating over the sequence  $\{\gamma_i\}$  in the outer loop.

A notable innovation in Algorithm 1 is the design of the stopping condition, which ensures that the uniform approximation errors of  $Q_i$  shrink progressively. This allows us to adapt the convergence proof from [24] to our inner loop, while proving the linear convergence rate of  $\{\gamma_i\}$  in the outer loop. Importantly, this design does not increase the time complexity of the inner loop.

We describe the details of the inner loop and the outer loop procedures of Algorithm 1 in the following:

- *Inner loop*: For each episode  $i$ , given a quotient coefficient  $\gamma_i$ , we perform an (arbitrary) Q-Learning algorithm (as the Speedy Q-Learning in [61]) to approximate function  $Q_{\gamma}^*(s, a)$  by  $Q_i(s, a)$ . Let  $s_0$  denote the initial state of any episode, and  $a_i \triangleq \arg \min_a Q_i(s_0, a)$  for all  $i \in [E] \triangleq \{1, \dots, E\}$ . We consider a *stopping condition*

$$\epsilon_i < -\alpha Q_i(s_0, a_i), \quad \forall i \in [E], \quad (20)$$

where  $\alpha > 0$  is the error scaling factor. This stopping condition ensures the algorithm being terminated in each episode  $i$  with a bounded *uniform approximation error*:  $\|Q_{\gamma}^* - Q_i\| \leq \epsilon_i, \forall i \in [E]$ . Operator  $\|\cdot\|$  is the supremum norm, which satisfies  $\|g\| \triangleq \max_{(s, a) \in \mathcal{Z}} g(s, a)$ . Specifically, we obtain  $Q_i(s_0, a_i)$ ,  $N_i(s_0, a_i)$ , and  $D_i(s_0, a_i)$ , which satisfy,

$$Q_i(s_0, a_i) = N_i(s_0, a_i) - \gamma_i D_i(s_0, a_i). \quad (21)$$

- *Outer loop*: We update the quotient coefficient:

$$\gamma_{i+1} = \mathbb{E}_{s_0 \sim \mu_0} \left[ \frac{N_i(s_0, a_i)}{D_i(s_0, a_i)} \right], \quad \forall i \in [E], \quad (22)$$

which will be shown to converge to the optimal value  $\gamma^*$ .

#### E. Convergence Analysis

We present the time complexity analysis of inner loop and the convergence results of our proposed FQL algorithm (Algorithm 1) as follows.

1) *Time Complexity of the inner loop*: Although as  $\{Q_i(s_0, a_i)\}$  is convergent to 0 and hence  $\epsilon_i < -\alpha Q_i$  is getting more restrictive as  $i$  increases, the steps needed  $T_i$  in Algorithm 1 keep to be finite without increasing over episode  $i$ . See [62, Appendix A] in detail.

2) *Convergence of FQL algorithm*: We then analyze the convergence of FQL algorithm:

**Theorem 1** (Linear Convergence of Fractional Q-Learning). *If the uniform approximation error  $\|Q_{\gamma_i}^* - Q_i\| \leq \epsilon_i$  holds with  $\epsilon_i < -\alpha Q_i(s_0, a_i)$  for some  $\alpha \in (0, 1)$  and for all  $i \in [E]$ , then the sequence  $\{\gamma_i\}$  generated by Algorithm 1 satisfies*

$$\frac{\gamma_{i+1} - \gamma^*}{\gamma_i - \gamma^*} \in (0, 1), \quad \forall i \in [E] \text{ and } \lim_{i \rightarrow \infty} \frac{\gamma_{i+1} - \gamma^*}{\gamma_i - \gamma^*} = \alpha. \quad (23)$$

*That is,  $\{\gamma_i\}$  converges to  $\gamma^*$  linearly.*

While the convergence proof in [24] requires obtaining the *exact* solution in each episode, Theorem 1 generalizes this result to the case where we only obtain an *approximated (inexact)* solution in each episode. In addition to the proof techniques in [24] and [61], our proof techniques include induction and exploiting the convexity of  $Q_i(s, a)$ . We present a proof sketch of Theorem 1 in [62, Appendix B].

The significance of Theorem 1 is two-fold. First, Theorem 1 shows that Algorithm 1 achieves a linear convergence rate, even though it only attains an approximation of  $Q_\gamma^*(s, a)$ . Second, (20) is a well-behaved stopping condition.

## V. FRACTIONAL MULTI-AGENT RL FRAMEWORK

In this section, we propose a fractional MARL framework with inexact Newton method, extending our fractional framework from the single-agent scenario to the multi-agent one. We first introduce a Markov game for our task scheduling problem. We then develop a fractional framework including fractional sub-games to address the fractional objective challenge. Finally, we propose the fractional Nash Q-learning algorithm and analyze the convergence of this algorithm to Nash equilibrium.

### A. Markov Game Formulation

We study our problem in a multi-agent scenario and introduce the task scheduling Markov game. The task scheduling Markov game is defined as:  $G = (M, \mathcal{S}, \mathcal{A}, \{c_{N,m}\}_{m=1}^M, \{c_{D,m}\}_{m=1}^M, \mathcal{P}, \delta, \mu_0)$  where  $M$  is the number of agents,  $\mathcal{S}$  and  $\mathcal{A}$  represent the state space and action space, respectively,  $\mathcal{P}(s'|s, a)$  denotes the state transition probability,  $\delta \in (0, 1)$  is discounted factor, and  $\mu_0$  denotes the initial state distribution.

We define the instant fractional costs at task  $k$  of mobile device  $m$  as

$$c_{N,m}(s_k, a_k) = A(Y_{m,k}, Z_{m,k+1}, Y_{m,k+1}), \quad (24)$$

$$c_{D,m}(s_k, a_k) = Y_{m,k} + Z_{m,k+1}. \quad (25)$$

Following the definition of discounted AoI in (6), we define the fractional long-term discounted cost for mobile device  $m$  as

$$V_m(s, \pi) = \frac{\mathbb{E}_\pi \left[ \sum_{k=0}^{\infty} \delta^k c_{N,m}(s_k, a_k) \middle| s_0 = s \right]}{\mathbb{E}_\pi \left[ \sum_{k=0}^{\infty} \delta^k c_{D,m}(s_k, a_k) \middle| s_0 = s \right]}, \quad (26)$$

where  $\pi = (\pi_m, \pi_{-m})$  represents the policies of mobile device  $m$  and other agents that determine actions, and  $\mathbb{E}_\pi$  is the expectation regarding transition dynamics given stationary control policy  $\pi$ . Note that (26) approximates the undiscounted function when  $\delta$  approaches 1 [63].

Specifically, an NE is a tuple of policies  $\pi^* = (\pi_m^*, \pi_{-m}^*)$  of game  $G$ . For each mobile  $m \in \mathcal{M}$ , given the fixed stationary policies  $\pi_{-m}^*$ , the fractional objective can be expressed as:

$$\pi_m^* = \arg \underset{\pi_m}{\text{minimize}} \quad V_m(s, \pi_m, \pi_{-m}^*), \quad \forall s \in \mathcal{S}. \quad (27)$$

Lemma 2 guarantees the existence of an NE in game  $G$ .

**Lemma 2.** *For the multi-player stochastic game with expected long-term discounted costs, there always exists a Nash equilibrium in stationary policies, where the probability of taking an action remains constant throughout the game [64].*

### B. Fractional Sub-Game

To deal with the fractional objective (27) for NE, we reformulated our game into iterative fractional sub-games based on Dinkelbach method [24] in this subsection.

First, we define sub-game  $G_\gamma$  with fractional coefficients  $\gamma$  for fractional sub-games as follows.

**Definition 2** (Fractional Sub-Game). *The fractional sub-game is defined as  $G_\gamma = (M, \mathcal{S}, \mathcal{A}, \{c_{N,m}\}_{m=1}^M, \{c_{D,m}\}_{m=1}^M, \mathcal{P}, \delta, \gamma)$ , where the new components are  $\gamma = \{\gamma_m\}_{m \in \mathcal{M}}$ , representing the set of Dinkelbach variables. Each  $\gamma_m$  is a Dinkelbach variable associated with mobile device  $m$ .*

The fractional value functions of sub-game are denoted as  $V_\gamma(s) := [V_{\gamma_m}(s)]_{m \in \mathcal{M}}$ . The value function for each mobile device  $m \in \mathcal{M}$  is given by

$$V_{\gamma_m}(s, \pi) = (1 - \delta) \cdot \mathbb{E}_\pi \left\{ \sum_{k=0}^{\infty} \delta^k [c_{N,m}(s_k, a_k) - \gamma_m c_{D,m}(s_k, a_k)] \middle| s_0 = s \right\}, \quad (28)$$

where  $s_k, a_k$  are the global state and action at task  $k$ .

In sub-game  $G_\gamma$ , each mobile device  $m$  aims to find its best response  $\pi_m^*$ . With policies of other agents  $\pi_{-m}^*$  fixed, the best response of mobile device  $m$  minimizes its cost value  $V_{\gamma_m}$  for any given global system state  $s \in \mathcal{S}$ . The objective is formulated as:

$$\pi_m^* = \arg \underset{\pi_m}{\text{minimize}} \quad V_{\gamma_m}(s, \pi_m, \pi_{-m}^*), \quad \forall s \in \mathcal{S}. \quad (29)$$

Lemma 2 ensures the existence of an NE in sub-game  $G_\gamma$ . For brevity, we denote the optimal state-value function as  $V_{\gamma_m}^*(s) = V_{\gamma_m}(s, \pi_m^*, \pi_{-m}^*), \forall s \in \mathcal{S}$ , where  $(\pi_m^*, \pi_{-m}^*)$  is the NE of sub-game  $G_\gamma$ .

Thus, we propose a fractional Nash Q-Learning algorithm based on the iterative fractional sub-games and show its convergence in the rest of this section.

### C. Fractional Nash Q-Learning Algorithm

We introduce the Fractional Nash Q-Learning (FNQL) algorithm in Algorithm 2. This algorithm includes two loops: 1) an inner loop that obtains NE of sub-game  $G_\gamma$ , and 2) an outer loop that iterates  $\gamma$  until convergence. The key idea is to iterate sub-game  $G_\gamma$  and attain the NE of Markov game  $G$  when  $\gamma$  converges.

1) *Inner Loop*: Following [65], we first define the Nash operator  $\mathbb{N}$  as follows:

**Definition 3** (Nash Operator). *Consider a collection of  $M$  functions,  $\mathbf{f}(\mathbf{a}) = [f_m(\mathbf{a}_m, \mathbf{a}_{-m})]_{m \in \mathcal{M}}$ , which admit a Nash equilibrium  $\pi^*$ . We introduce the Nash operator  $\mathbb{N}_{\mathbf{a} \in \mathcal{A}}$ , which maps the collections of functions into their corresponding Nash equilibrium values, i.e.,  $\mathbf{f}(\mathbf{a}^*) = \mathbb{N}_{\mathbf{a} \in \mathcal{A}} \mathbf{f}(\mathbf{a})$ , satisfying*

$$f_m(\mathbf{a}_m^*, \mathbf{a}_{-m}^*) \leq f_m(\mathbf{a}_m, \mathbf{a}_{-m}^*), \quad \forall \mathbf{a}_m, \forall m \in \mathcal{M}. \quad (30)$$

For sub-game  $G_\gamma$ , the optimization of best response (29) utilize an instant cost, given by  $c_{N_m}(\mathbf{s}, \mathbf{a}) - \gamma_m c_{D_m}(\mathbf{s}, \mathbf{a}), \forall m \in \mathcal{M}$ . To solve this optimization, we apply the traditional MARL algorithm Nash Q-learning [25].

*Nash-Q Functions*. We define the Nash Q-functions with  $\gamma$  as:

$$\mathbf{Q}_\gamma(\mathbf{s}, \mathbf{a}) \triangleq \mathbf{c}_N(\mathbf{s}, \mathbf{a}) - \gamma \odot \mathbf{c}_D(\mathbf{s}, \mathbf{a}) + \delta \mathbb{E}_{\mathcal{P}} \left[ \mathbb{N}_{\mathbf{a} \in \mathcal{A}} \mathbf{Q}_\gamma(\mathbf{s}, \mathbf{a}) \right], \quad (31)$$

where  $\odot$  stands for the element-wise product of two vectors. We denote  $\mathbf{c}_N(\mathbf{s}, \mathbf{a}) = [c_{N_m}(\mathbf{s}, \mathbf{a})]_{m \in \mathcal{M}}$ ,  $\mathbf{c}_D(\mathbf{s}, \mathbf{a}) = [c_{D_m}(\mathbf{s}, \mathbf{a})]_{m \in \mathcal{M}}$ . We use  $\mathbb{E}_{\mathcal{P}}$  as a shorthand notation for  $\mathbb{E}_{\mathbf{s}' \sim \mathcal{P}(\cdot | \mathbf{s}, \mathbf{a})}$ . In the inner loop, we update the Q-function of mobile device  $m \in \mathcal{M}$  at iteration  $k$  by

$$\begin{aligned} \mathbf{Q}_\gamma^{k+1}(\mathbf{s}, \mathbf{a}) = & (1 - \lambda) \mathbf{Q}_\gamma^k(\mathbf{s}, \mathbf{a}) + \lambda \{ \mathbf{c}_N(\mathbf{s}, \mathbf{a}) - \gamma \odot \mathbf{c}_D(\mathbf{s}, \mathbf{a}) \\ & + \delta \mathbb{E}_{\mathcal{P}} \left[ \mathbb{N}_{\mathbf{a} \in \mathcal{A}} \mathbf{Q}_\gamma^k(\mathbf{s}', \mathbf{a}) \right] \}, \end{aligned} \quad (32)$$

where  $\lambda$  is the learning rate. We observe that the Nash Q-function in (31) is the fixed point of the iteration in (32).

*Nash Equilibrium Policies*. Let  $\pi_\gamma^*(\mathbf{s}) = [\pi_m^*(\mathbf{s})]_{m \in \mathcal{M}}$  be the NE policies of the sub-game  $G_\gamma$ . We have that

$$\pi_{\gamma, m}^*(\mathbf{s}) = \arg \min_{\mathbf{a}_m} Q_{\gamma, m}(\mathbf{s}, \mathbf{a}_m), \quad \forall m \in \mathcal{M}. \quad (33)$$

*Value functions*. We define  $\bar{N}_\gamma^*(\mathbf{s}) = [\bar{N}_{\gamma, m}^*(\mathbf{s})]_{m \in \mathcal{M}}$  and  $\bar{D}_\gamma^*(\mathbf{s}) = [\bar{D}_{\gamma, m}^*(\mathbf{s})]_{m \in \mathcal{M}}$  as the numerator numerator value functions and denominator value functions as follows

$$\bar{N}_\gamma^*(\mathbf{s}) \triangleq \mathbf{c}_N(\mathbf{s}, \pi_\gamma^*(\mathbf{s})) + \delta \mathbb{E}_{\mathbf{s}' \sim \mathcal{P}(\cdot | \mathbf{s}, \pi_\gamma^*(\mathbf{s}))} [\bar{N}_\gamma^*(\mathbf{s}')], \quad (34)$$

$$\bar{D}_\gamma^*(\mathbf{s}) \triangleq \mathbf{c}_D(\mathbf{s}, \pi_\gamma^*(\mathbf{s})) + \delta \mathbb{E}_{\mathbf{s}' \sim \mathcal{P}(\cdot | \mathbf{s}, \pi_\gamma^*(\mathbf{s}))} [\bar{D}_\gamma^*(\mathbf{s}')]. \quad (35)$$

It follows from (31) that  $\mathbb{N}_{\mathbf{a} \in \mathcal{A}} \mathbf{Q}_\gamma(\mathbf{s}, \mathbf{a}) = \bar{N}_\gamma^*(\mathbf{s}) - \langle \gamma, \bar{D}_\gamma^*(\mathbf{s}) \rangle$ . We approximate the Nash operator  $\mathbb{N}_{\mathbf{a} \in \mathcal{A}}$  as detailed in [62, Appendix C].

For each sub-game  $G_\gamma$ , we perform the fractional Nash Q-Learning algorithm to obtain the Nash Q-functions  $\mathbf{Q}_\gamma(\mathbf{s})$ . Each episode terminates when the Nash equilibrium of sub-game  $G_\gamma$  is attained.

---

**Algorithm 2** Fractional Nash Q-Learning (FNQL)

---

```

1: Initialize a tolerance coefficient  $\epsilon$ ;
2: repeat
3:   for  $k = 0, 1, \dots, K$  do
4:     Initialize  $\mathbf{s}_0$ ;
5:     Choose action  $\mathbf{a}$  based on current  $\mathbf{Q}^k$ ;
6:     Observe  $\mathbf{c}_N, \mathbf{c}_D, \mathbf{a}$ , and  $\mathbf{s}'$ ;
7:     Update  $\mathbf{Q}_\gamma^k$  by (32);
8:   end for
9:   Update  $\gamma_m$  by (40) for all  $m \in \mathcal{M}$ ;
10:  until  $\|\mathbb{E}_{\mathbf{s}_0 \sim \mu_0} [\bar{N}_\gamma^*(\mathbf{s}_0) - \langle \gamma, \bar{D}_\gamma^*(\mathbf{s}_0) \rangle]\| \leq \epsilon$ .

```

---

2) *Outer loop*: Given  $\gamma \in \Gamma$ , we utilize neural networks (detailed in Section VI) to approximate the Nash Equilibrium strategy  $\pi_{\gamma, m}^*$  for each player  $m \in \mathcal{M}$  in sub-game  $G_\gamma$ . Let  $\theta_m(\gamma) \in \Theta_m$  denote the parameters of the neural network trained for player  $m$  given  $\gamma$ . We define the mapping  $\theta : \Gamma \rightarrow \Theta$ , where  $\Theta = \times_{m \in \mathcal{M}} \Theta_m$ . The outputs of these neural networks, parameterized by  $\theta(\gamma)$ , collectively approximate the NE strategy profile  $\pi_\gamma^*$  for the sub-game  $G_\gamma$ . Based on the strategies parameterized by  $\theta$ , we define the following expected value functions for agent  $m$ :

$$N_m(\theta, \gamma_m) = \mathbb{E}_{\mathbf{s}_0 \sim \mu_0} [\bar{N}_{\gamma_m}^*(\mathbf{s}_0)], \quad (36)$$

$$D_m(\theta, \gamma_m) = \mathbb{E}_{\mathbf{s}_0 \sim \mu_0} [\bar{D}_{\gamma_m}^*(\mathbf{s}_0)], \quad (37)$$

$$F_m(\theta, \gamma_m) = \mathbb{E}_{\mathbf{s}_0 \sim \mu_0} [\bar{N}_{\gamma_m}^*(\mathbf{s}_0) - \gamma_m \bar{D}_{\gamma_m}^*(\mathbf{s}_0)]. \quad (38)$$

We denote the objective functions  $\mathbf{F}(\theta, \gamma) = [F_m(\theta, \gamma_m)]_{m \in \mathcal{M}}$ . For simplicity, let  $\theta^* = \theta(\gamma^*)$ , which represents the parameters for the NE strategy of original Markov game  $\mathbf{G}$ . We establish the existence of an equivalent condition of reaching NE between the Markov game  $\mathbf{G}$  and the fractional sub-game  $G_\gamma$  with the following lemma:

**Lemma 3.** *There exists  $\gamma^* \succ 0$ , such that the NE strategy  $\pi^*$  of game  $\mathbf{G}$  is also an NE strategy of sub-game  $G_{\gamma^*}$ . For  $\gamma^*$ , the corresponding  $\mathbf{F}(\theta^*, \gamma^*)$  satisfies:*

$$\mathbf{F}(\theta^*, \gamma^*) = \mathbf{0}. \quad (39)$$

Lemma 3 is proven using the property of (31) and the Brouwer fixed point theorem. The detailed proof can be found in [62, Appendix D].

The outer loop implements the iterations of fractional sub-game based on generalizing the Dinkelbach method [24]. At each iteration  $i$ , after achieving the NE of sub-game  $G_{\gamma_i}$ , we update coefficients  $\gamma$  in line 9 of Algorithm 2 as

$$\gamma_{m, i+1} = \frac{N_m(\theta, \gamma_{m, i})}{D_m(\theta, \gamma_{m, i})}, \quad \forall m \in \mathcal{M}. \quad (40)$$

We repeat this process until  $\gamma$  converges, which happens when  $\mathbb{E}_{\mathbf{s}_0 \sim \mu_0} [\bar{N}_\gamma^*(\mathbf{s}_0) - \gamma \bar{D}_\gamma^*(\mathbf{s}_0)]$  is sufficiently close to 0. We proceed to show that the updates in (40) constitutes an inexact Newton's method and quantify the conditions that lead to a linear convergence rate for the outer loop.

#### D. Convergence Analysis of Outer Loop

We analyze the convergence properties of the outer loop by establishing the connection between the update rule (40) and the Newton's method. The outer loop aims to find the root of the function  $\gamma \mapsto \mathbf{F}(\boldsymbol{\theta}(\gamma), \gamma) = \mathbf{0}$ , where  $\boldsymbol{\theta}(\gamma)$  represents the parameters of the NE strategy for the sub-game  $G_\gamma$ . Thus, we consider the Jacobian of  $\mathbf{F}(\boldsymbol{\theta}, \gamma)$  with respect to  $\gamma$ . Specifically, the  $(m, n)$ -th entry of the Jacobian is given by:

$$[J_{\mathbf{F}}(\boldsymbol{\theta}, \gamma)]_{mn} = \sum_{k \neq m} \nabla_{\boldsymbol{\theta}_k} F_m(\boldsymbol{\theta}_m, \gamma_m) \frac{\partial \boldsymbol{\theta}_k(\boldsymbol{\theta})}{\partial \gamma_n} - \delta_{mn} D_m(\boldsymbol{\theta}_m, \gamma_m), \quad (41)$$

where  $\delta_{mn}$  is defined as

$$\delta_{mn} = \begin{cases} 1, & \text{if } m = n, \\ 0, & \text{if } m \neq n. \end{cases}$$

We start by analyzing a simplified scenario: the single-agent case without inter-agent dependencies. In this case, the Jacobian simplifies to a diagonal form:

$$[J'_{\mathbf{F}}(\boldsymbol{\theta}, \gamma)]_{mm} = -D_m(\boldsymbol{\theta}_m, \gamma_m). \quad (42)$$

Provided the required derivatives are non-zero, the update rule (40) for agent  $m$  in the exact Newton's method step for a single-agent case is

$$\begin{aligned} \gamma_{m,i+1} &= \gamma_{m,i} - [J'_{\mathbf{F}}(\boldsymbol{\theta}, \gamma_i)]_{mm}^{-1} F_m(\boldsymbol{\theta}_m, \gamma_{m,i}) \\ &= \frac{N_m(\boldsymbol{\theta}, \gamma_{m,i})}{D_m(\boldsymbol{\theta}, \gamma_{m,i})} \end{aligned} \quad (43)$$

That is, the single-objective (single-agent) Dinkelbach's method is equivalent to the Newton's method, and hence the sequence  $\{\gamma_{m,i}\}$  converges quadratically to  $\gamma_m^*$ .

However, generating to the multi-agent scenario introduces significant theoretical and computational challenges, as it is difficult to compute  $\frac{\partial \boldsymbol{\theta}_k(\boldsymbol{\theta})}{\partial \gamma_n}$  in the Jacobian (41). For the multi-agent scenario, we consider the update rule (40) within the framework of the inexact Newton method. The inexact Newton method is characterized by the following convergence conditions.

**Lemma 4.** *Let  $\mathbf{L} : \mathbb{R}^n \rightarrow \mathbb{R}^n$  be a continuously differentiable function with a solution  $\mathbf{x}^*$  where  $\mathbf{L}'(\mathbf{x}^*)$  is nonsingular. The inexact Newton iteration  $\mathbf{x}_{i+1} = \mathbf{x}_i + \mathbf{s}_i$  and  $\mathbf{L}'(\mathbf{x}_i)\mathbf{s}_i = -\mathbf{L}(\mathbf{x}_i) + \mathbf{r}_i$ , converges linearly to  $\mathbf{x}^*$  if  $\|\mathbf{r}_i\| \leq \eta_i \|\mathbf{L}(\mathbf{x}_i)\|$  for  $0 \leq \eta_i \leq \eta_{\max} < 1$ , provided  $\mathbf{x}_0$  is sufficiently close to  $\mathbf{x}^*$  [66].*

In our context, the update step  $\mathbf{s}_i = \gamma_{i+1} - \gamma_i$  for the game  $G$  can be viewed as the *inexact* Newton equation:

$$\mathbf{J}_{\mathbf{F}}(\boldsymbol{\theta}, \gamma_i)\mathbf{s}_i = -\mathbf{F}(\boldsymbol{\theta}, \gamma_i) + \mathbf{r}_i, \quad (44)$$

where  $\mathbf{r}_i$  is the residual term. This allows us to adapt convergence analysis of inexact Newton method [66] to our multi-agent framework.

To establish convergence when employing an *inexact* Newton method, we require several assumptions regarding the structure of the problem near the equilibrium. These assumptions essentially ensure that the local landscape of the game is sufficiently well-behaved and interactions between agents are appropriately bounded. We define an open neighborhood  $\mathcal{N}_{\gamma^*}$  around  $\gamma^*$  and the subsequent assumptions hold uniformly for all  $\gamma \in \mathcal{N}_{\gamma^*}$ .

The first assumption guarantees desirable curvature properties for each agent's local objective component, related to the block-diagonal part of the Hessian of  $\mathbf{F}$  with respect to  $\boldsymbol{\theta}$ . We denote this Hessian as  $H := \nabla_{\boldsymbol{\theta}}^2 \mathbf{F}(\boldsymbol{\theta}, \gamma)$ .

**Assumption 1** (Bounded Inverse of Local Hessian Block).

$$\text{For each } m \in \mathcal{M}, \text{ we have } \|(H_{\boldsymbol{\theta}_m \boldsymbol{\theta}_m})^{-1}\|_{\infty} \leq 1/\mu.$$

This assumption is a standard condition in optimization that prevents the Hessian blocks  $H_{\boldsymbol{\theta}_m \boldsymbol{\theta}_m}$ , which are related to each agent's local optimization problem, from being singular or near-singular.

We then impose conditions on the denominator term appearing in the average AoI metric, ensuring it is well-behaved and its gradient is bounded.

**Assumption 2** (Bounded Denominator and Gradient). *For all  $m \in \mathcal{M}$ ,  $D_m(\boldsymbol{\theta}, \gamma_m)$  is uniformly bounded below by  $D_{\min} > 0$ , i.e.,  $D_m(\boldsymbol{\theta}, \gamma_m) \geq D_{\min} > 0$ . Additionally, the norm of the gradient of  $D_m$  with respect to  $\boldsymbol{\theta}_m$  is bounded:  $\|\nabla_{\boldsymbol{\theta}_m} D_m(\boldsymbol{\theta}, \gamma_m)\|_{\infty} \leq C_D$ .*

This assumption prevents division by zero or numerically unstable small values in the objective function  $F_m$ , ensuring it remains well-defined and finite. The bound  $C_D$  on the gradient limits the sensitivity of the denominator to changes in  $\boldsymbol{\theta}_m$ .

We also need to control the strength of interactions between different agents.

**Assumption 3** (Bounded Interaction). *For all  $k \neq m$ , the norm of the first and second order cross-gradients of  $F_m$  is bounded as  $\|\nabla_{\boldsymbol{\theta}_k} F_m(\boldsymbol{\theta})\|_{\infty} \leq C_{\text{int}}$  and  $\|H_{\boldsymbol{\theta}_k \boldsymbol{\theta}_m}\| = \|\nabla_{\boldsymbol{\theta}_k \boldsymbol{\theta}_m}^2 F_m(\boldsymbol{\theta}, \gamma_m)\|_{\infty} \leq H_{\text{int}}$  for all  $m, k$ . For each agent  $m$ , the number of other agents  $k \neq m$  is bounded as:  $|\mathcal{N}_m^{\text{grad}}| := |\{k \neq m \mid \nabla_{\boldsymbol{\theta}_k} F_m(\boldsymbol{\theta}, \gamma) \neq 0\}| \leq K_{\text{grad}}$ . Similarly, the number of subsystems  $l$  influencing agent  $k$  through the Hessian term is bounded by  $|\{k \neq m \mid H_{\boldsymbol{\theta}_k \boldsymbol{\theta}_m} \neq 0\}| \leq K_{\text{hess}}$ . We define  $K = \max(K_{\text{grad}}, K_{\text{hess}})$  and assume  $K$  is a constant independent of the system size  $M$ .*

This assumption quantifies the coupling among agents by positing that the direct marginal effect of agent  $k$ 's parameters  $\boldsymbol{\theta}_k$  on agent  $m$ 's objective  $F_m$  is bounded. This is a common and reasonable assumption in large systems, reflecting localized rather than global influence. It implies each agent is directly influenced by only a limited number  $K$  of others, independent of the total system size  $M$ . This reasonably models systems like MEC, where agents (e.g., mobile devices) have limited communication ranges [67].

Based on Lemma 4 and Assumptions 1-3, we are ready to present the convergence result for Algorithm 2 applied to game  $G$ :

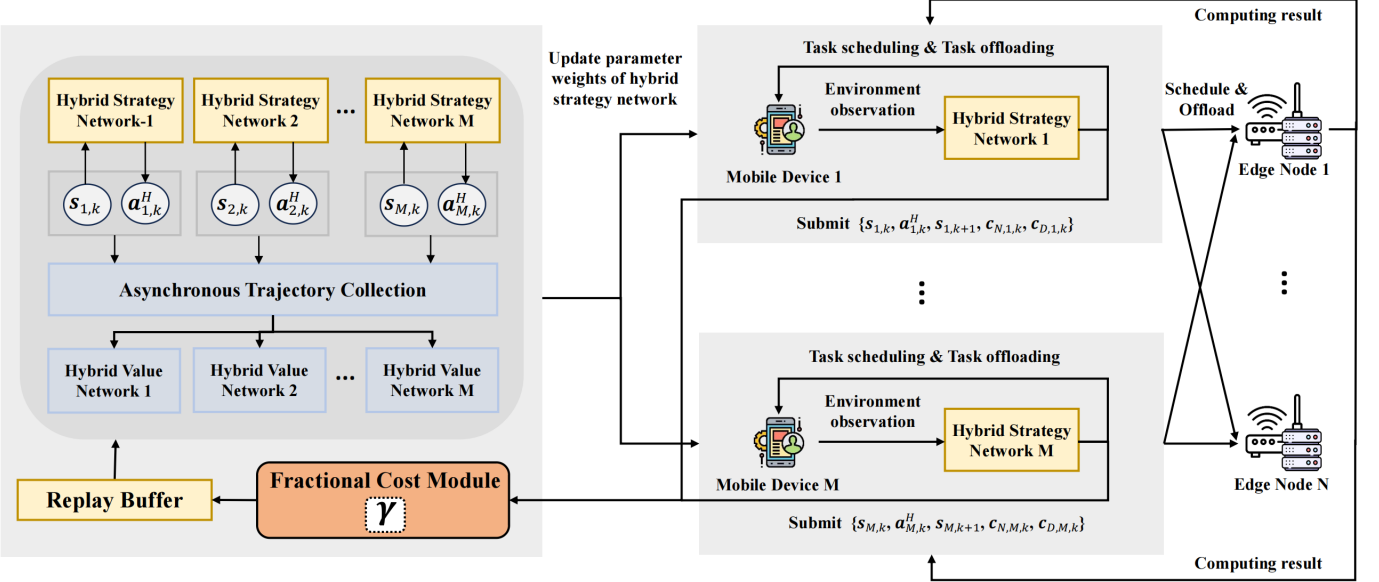


Fig. 2. Illustration on the proposed asynchronous fractional MADRL framework with fractional cost module, asynchronous trajectory collection mechanism, and hybrid strategy and value networks with R-D3QN and R-PPO.

**Theorem 2** (Linear Convergence of Outer Loop). *Assuming Assumptions 1-3 hold, the initial  $\gamma_0$  is sufficiently close to  $\gamma^*$ , and the conditions  $\frac{KH_{int}}{\mu} < 1$  and  $\frac{C_D C_{int}}{D_{min}(1/K - H_{int})} < 1$  are satisfied, then Algorithm 2 using the inexact Newton step characterized by (44) converges linearly to a Nash Equilibrium of game  $\mathbf{G}$ .*

Please refer to [62, Appendix E] for a detailed proof. Analyzing the convergence of the outer loop, which involves the multi-agent interactions and the inexact Newton method, constitutes a key contribution of this work in Theorem 2. This analysis is achieved under reasonable and justifiable assumptions about the problem structure.

## VI. ASYNCHRONOUS FRACTIONAL MADRL ALGORITHM

In this section, we introduce A. F. MADRL, an asynchronous fractional MADRL algorithm. This algorithm achieves NE for the SMG Problem (8) with hybrid action space, as shown in Fig. 2.

Building on the fractional MARL framework proposed in Section V, we first introduce a fractional cost module of  $\gamma$ . This module approximates NE when optimizing the fractional AoI objective in multi-agent scenario. However, when considering the scheduling problem of MEC formulated as SMG, synchronized decision-making and training become inefficient due to asynchronous task completions. To address the challenge of asynchronous decision-making, we introduce an asynchronous trajectory collection mechanism. Additionally, we propose the corresponding hybrid strategy and value networks to apply the mechanism for hybrid action spaces of updating and offloading actions.

### A. Fractional Cost Module

As in the proposed fractional MARL framework in Section V, we consider a set of episodes  $i \in [E]$  and introduce a quotient coefficient  $\gamma_i$  for episode  $i$ . We define  $\mathbf{a}_i^H = [\mathbf{a}_{m,i}^H]_{m=1}^M$ ,

where  $\mathbf{a}_{m,i}^H \triangleq [(\mathbf{a}_m^U, \mathbf{a}_m^O)]_{k=1}^K$  as the set of updating and offloading strategies of mobile device  $m \in \mathcal{M}$  in episode  $i$ , where superscript ‘H’ refers to ‘history’.

At each task  $k$ , we determine a fractional cost and send it for training. This process corresponds to the sub-game of the proposed fractional RL framework. Based on (29), we define the cost for all  $i \in [E], m \in \mathcal{M}$ , and  $k \in \mathcal{K}$  as:

$$c_{m,k}^i(\mathbf{a}_m^H, \mathbf{a}_{-m}^H) = A_m(Y_{m,k}^i, Z_{m,k+1}^i, Y_{m,k+1}^i) - \gamma_m \cdot (Y_{m,k}^i + Z_{m,k+1}^i), \quad (45)$$

where for episode  $i$ ,  $Y_{m,k}^i$  denotes the duration of task  $k$ ,  $Z_{m,k+1}^i$  is the waiting time before generating task  $k+1$ , and  $A(Y_{m,k}^i, Z_{m,k+1}^i, Y_{m,k+1}^i)$  represents the trapezoid area in (4). Note that  $Y_{m,k}$  is a function of  $\mathbf{a}_m^U$ , and  $Z_{m,k+1}$  is a function of  $(\mathbf{a}_m^H, \mathbf{a}_{-m}^H)$ . The fractional cost module tracks  $(\mathbf{a}_m^H, \mathbf{a}_{-m}^H)$ , or equivalently  $Y_{m,k}$  and  $Z_{m,k}$  for all  $k = 0, 1, \dots, K$  throughout the training process.

Finally, at the end of each episode  $m$ , the fractional cost module updates  $\gamma_{m,i+1}$  by:

$$\gamma_m^{i+1} = \frac{\sum_{k=0}^K \delta^k A_m(Y_{m,k}^i, Z_{m,k+1}^i, Y_{m,k+1}^i)}{\sum_{k=0}^K \delta^k (Y_{m,k}^i + Z_{m,k+1}^i)}. \quad (46)$$

### B. Asynchronous Trajectory Collection Mechanism

Our framework utilize the CTDE paradigm to support asynchronous actions by decoupling execution from training. Specifically, we propose an asynchronous central mechanism that aggregates agent trajectories aligned via a global event index  $T$ . This globally consistent information is then leveraged to train the agents’ policy and value networks.

We compare our asynchronous mechanism with traditional MARL and VarlenMARL [49], an asynchronous MADRL algorithm, in the following example:

- Traditional MADRL algorithms such as MADDPG [21] and MAPPO require synchronous joint information from all agents at each time step, making them unsuitable for asynchronous decision-makings. Traditional MARL algorithms gather joint data from all agents at each time step. The collected joint trajectory is

$$[(s_1, a_{1,1}, a_{2,1}), (s_2, a_{1,2}, a_{2,2}), (s_3, a_{1,3}, a_{2,3}), \dots]. \quad (47)$$

- VarlenMARL [49], an asynchronous MADRL algorithm, addresses this by allowing variable-length trajectories. However, it still struggles to fully utilize agent interactions in asynchronous environments. It allows agents to collect trajectories asynchronously. It merges an agent's data with the latest padded data from other agents. Let  $s_m^0, a_m^0$  be the initial trajectory of agent  $m$ . Fig. 3(a) shows the trajectories of Agents 1 and 2 as:

$$[(s_{1,1}, a_{1,1}, (s_{2,0}, a_{2,0})), (s_{1,2}, a_{1,2}, (s_{2,1}, a_{2,1})), (s_{1,3}, a_{1,3}, (s_{2,1}, a_{2,1})) \dots], [(s_{2,1}, a_{2,1}, (s_{1,1}, a_{1,1})), (s_{2,2}, a_{2,2}, (s_{1,3}, a_{1,3})), (s_{2,3}, a_{2,3}, (s_{1,3}, a_{1,3})), \dots].$$

- Our proposed asynchronous trajectory collection mechanism, illustrated in Fig. 3(b), addresses these limitations. It operates based on a global event sequence managed by the centralized controller. Let  $(s_T, a_T)$  denote the state-action pair associated with the  $T$ -th global (originating from some agent  $m_T$ ). To capture the history of interactions among agents, we introduce the time-aggregated history state,  $H_T \in \mathbb{R}^d$ .  $H_T$  is a fixed-dimensional vector that serves as a summary representation derived from the sequence of all state-action pairs corresponding to global events from 1 to  $T-1$ . This history state is updated sequentially using a history aggregation transition function, denoted as  $TA$ . Upon receiving the  $T$ -th state-action pair  $(s_T, a_T)$ , the controller computes the subsequent history state  $H_{T+1}$  via the update rule:

$$H_{T+1} = TA((s_T, a_T), H_T) \quad (48)$$

where  $TA : (\mathcal{S} \times \mathcal{A}) \times \mathbb{R}^d \rightarrow \mathbb{R}^d$  represents the transition function that maps the current event's state-action information and the previous history state to the new history state. In our implementation,  $TA$  corresponds to the state transition function of a Gated Recurrent Unit (GRU) network [68], processing an embedding of the input pair  $(s_T, a_T)$  and the previous hidden state  $H_T$  to produce the new hidden state  $H_{T+1}$ . Implementation details of the RNN networks are provided in Appendix F [62]. The resulting collected trajectory is a sequence ordered by the global event index  $T$ , as shown in Fig. 3(b):

$$[(s_{1,1}, a_{1,1}, H_1), (s_{2,1}, a_{2,1}, H_2), (s_{1,2}, a_{1,2}, H_3), (s_{1,3}, a_{1,3}, H_4), (s_{2,2}, a_{2,2}, H_5), (s_{2,3}, a_{2,3}, H_6), \dots].$$

This mechanism facilitates more accurate evaluations of states and  $Q$  values by leveraging global states, actions, and the aggregated information derived from all agents' prior action.

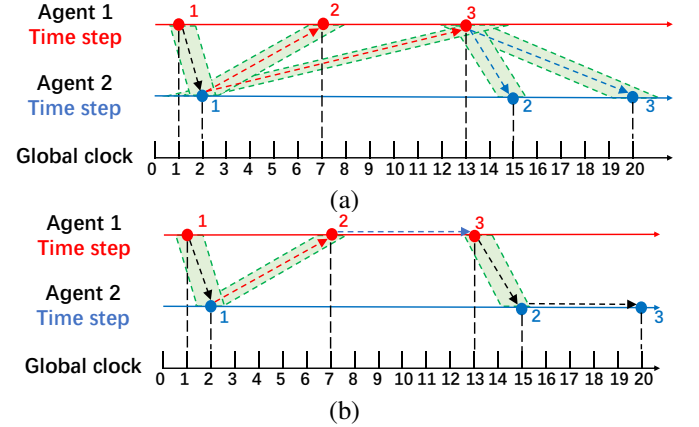


Fig. 3. Comparison of trajectory collection mechanisms under VarlenMARL, and our proposed RNN-PPO. (a) In VarlenMARL, an agent collects its trajectory as well as the latest information from other agents. (b) In RNN-PPO, agent collects its trajectory with the time-aggregating information from history decision events.

### C. Hybrid Strategy Network

Our algorithm employs independent learners to train hybrid strategy and value networks for each device asynchronously. Within the CTDE framework, each agent inputs both local observations and a shared time-aggregated history (RNN hidden state) from the central trainer.<sup>3</sup>

The asynchronous trajectory collection mechanism synthesizes time-aggregating data. It utilizes state-action pairs from other agents and historical events to improve agent interactions. We implement this mechanism with a GRU, forming the RNN-D3QN (R-D3QN) and RNN-PPO (R-PPO) architectures for discrete and continuous actions, respectively. Please refer to Appendix F for details. On a central server, the collected asynchronous trajectories are sampled to perform synchronous parameter updates for all agents' networks. The resulting off-policy learning challenge is stabilized by the inherent design of our DRL algorithms (e.g., importance sampling in PPO) and by conditioning updates on the aggregated historical context from the GRU. These hybrid networks address both the task offloading and updating processes.

## VII. PERFORMANCE EVALUATION

We evaluate our fractional multi-agent framework with experiments involving 20 mobile devices. Our experimental setup follows the settings outlined in [12, Table I], with key experiment settings and parameters provided in [62, Appendix G]. We compare our proposed algorithms and baseline algorithms as follows.

- Non-Fractional MADRL (denoted by Non-F. MADRL):* This benchmark lets each mobile device learn hybrid DRL algorithms individually, without a fractional scheme. The algorithm leverages D3QN to generate discrete offloading decisions, while employing PPO to produce continuous updating decisions. In comparison to our proposed fractional framework, this benchmark

<sup>3</sup>We centrally train the hybrid networks in a trusted third-party.

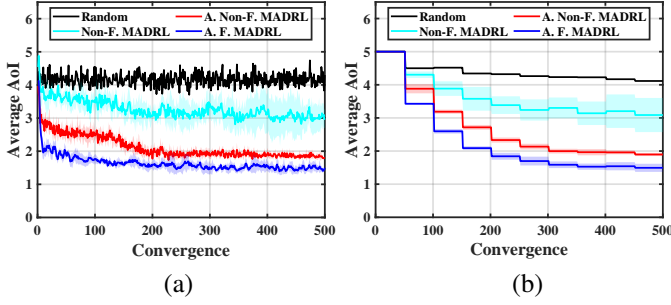


Fig. 4. Convergence of (a) average AoI and (b) the exponential moving average values of (Dinkelbach) quotient coefficients  $\gamma$  across devices, where  $\gamma$  is updated every 50 episodes. The unit of AoI is measured in seconds.

is non-fractional and lacks the asynchronous trajectory collection mechanism. It approximates the ratio-of-expectation average AoI by an expectation-of-ratio expression:  $\text{minimize}_{\pi_m} \mathbb{E} \left[ \frac{A(Y_{m,k}, Z_{m,k+1}, Y_{m,k+1})}{Y_{m,k} + Z_{m,k+1}} \mid \pi_m \right]$ . This approximation to tackle the fractional challenge tends to cause large accuracy loss.

- **Asynchronous Non-Fractional MADRL (denoted by A. Non-F. MADRL):** This benchmark incorporates the asynchronous trajectory collection mechanism into the Non-F. MADRL algorithm to demonstrate its effectiveness. While it employs the same asynchronous trajectory collection mechanism as our proposed A. F. MADRL algorithm, it lacks the fractional framework.
- **A. F. MADRL:** The proposed A. F. MADRL algorithm incorporates two key elements. First, it uses a fractional scheme to approximate the NE. Second, it employs a trajectory collection mechanism, which aggregates information from both historical records and other agents.
- **Random:** This method randomly schedules updating and offloading decisions within the action spaces.
- **H-MAPPO:** Multi-agent proximal policy optimization [23] with hybrid action spaces.
- **VarlenMARL:** VarLenMARL [49] implements independent time steps with variable lengths for each agent. It utilizes a synchronized delay-tolerant mechanism to enhance performance. This approach is discussed in Section II and VI.
- **F. DRL:** Fractional DRL (F. DRL) [1] adapts fractional framework based on Dinkelbach method on DRL algorithms without considering the multi agent scenario.
- **HAPPO:** Heterogeneous-Agent Proximal Policy Optimisation (HAPPO) algorithms [69] with hybrid action spaces.
- **PGOW:** Potential-game-inspired offloading & waiting baseline (PGOW) that combines  $\epsilon$ -greedy best-response offloading with log-linear learning for waiting. The offloading strategy considers estimated service time and queue-dependent congestion. These dynamics are standard in potential game settings [70], [71].
- **ASM:** Asynchronous and Scalable Multi-agent Proximal Policy Optimization (ASM-PPO) [51] allows asynchronous learning and decision-making based on PPO.

Our experiments first evaluate the convergence of our pro-

posed algorithms. We then compare their performance against baselines. The average AoI at the evaluation is computed using the following equation:

$$\Delta_m = \frac{\sum_{k=0}^K A_m(Y_{m,k}, Z_{m,k+1}, Y_{m,k+1})}{\sum_{k=0}^K (Y_{m,k} + Z_{m,k+1})}. \quad (49)$$

Our experiments systematically evaluate the impacts of several factors: edge capacity, drop coefficient, task density, mobile capacity, processing variance, and number of agents.

**Convergence:** Fig. 4 illustrates the convergence result of the Non-F. DRL algorithm, as well as proposed A. Non-F. MADRL and A. F. MADRL algorithms. We examine two key aspects: the convergence of the average AoI and that of the average fractional coefficient,  $\gamma$ , which should converge concurrently.

In Fig. 4(a), both A. Non-F. MADRL and A. F. MADRL algorithms are shown to converge after approximately 300 episodes. Notably, A. F. MADRL achieves a 50.6% reduction in converged average AoI compared to Non-F. DRL, demonstrating the efficacy of the proposed fractional framework. Furthermore, the performance difference between A. F. MADRL and A. Non-F. MADRL shows the substantial impact of the asynchronous trajectory collection mechanism. On the other hand, the random scheme in fact cannot converge. Instead, the average value in Fig. 4(b) gradually approached its average AoI in Fig. 4(a), starting from its initial value.

**Edge Capacity:** In Fig. 5(a), we evaluate different processing capacities of edge servers. The use of the fractional cost module in A. F. MADRL results in an average AoI reduction of 31.1% compared to the A. Non-F. MADRL approach. The proposed A. F. MADRL algorithm consistently achieves smaller average AoI compared to other benchmarks that don't consider fractional AoI and asynchronous settings. A. F. MADRL reduces the average AoI by up to 21.9% compared with F. DRL at 35 GHz. We observe that the performance gap between the proposed A. F. MADRL and other baseline schemes becomes more pronounced when the edge capacity is limited. These results demonstrate that an optimized design tailored for asynchronous settings can achieve superior performance, especially in resource-constrained environments.

**Drop Coefficient:** Fig. 5(b) illustrates the results of different drop coefficients, which are the ratios of drop time  $\bar{Y}$  to the task processing duration. While the average AoI of random scheduling decreases as the drop coefficient increases, other RL techniques show no clear trend. This suggests that the updating policy may serve as a dropping mechanism. With different drop coefficients, our proposed A. F. MADRL algorithm achieves approximately 33.8% less average AoI compared against H-MAPPO on average.

**Task Density:** Fig. 5(c) shows the AoI performance under varying task densities. These densities affect overall task loads and expected processing duration at mobile devices and edge servers. Non-A. F. MADRL outperforms Non-F. MADRL by 37.7% on average. Additionally, our A. F. MADRL algorithm outperforms all other benchmarks. At high task density (65

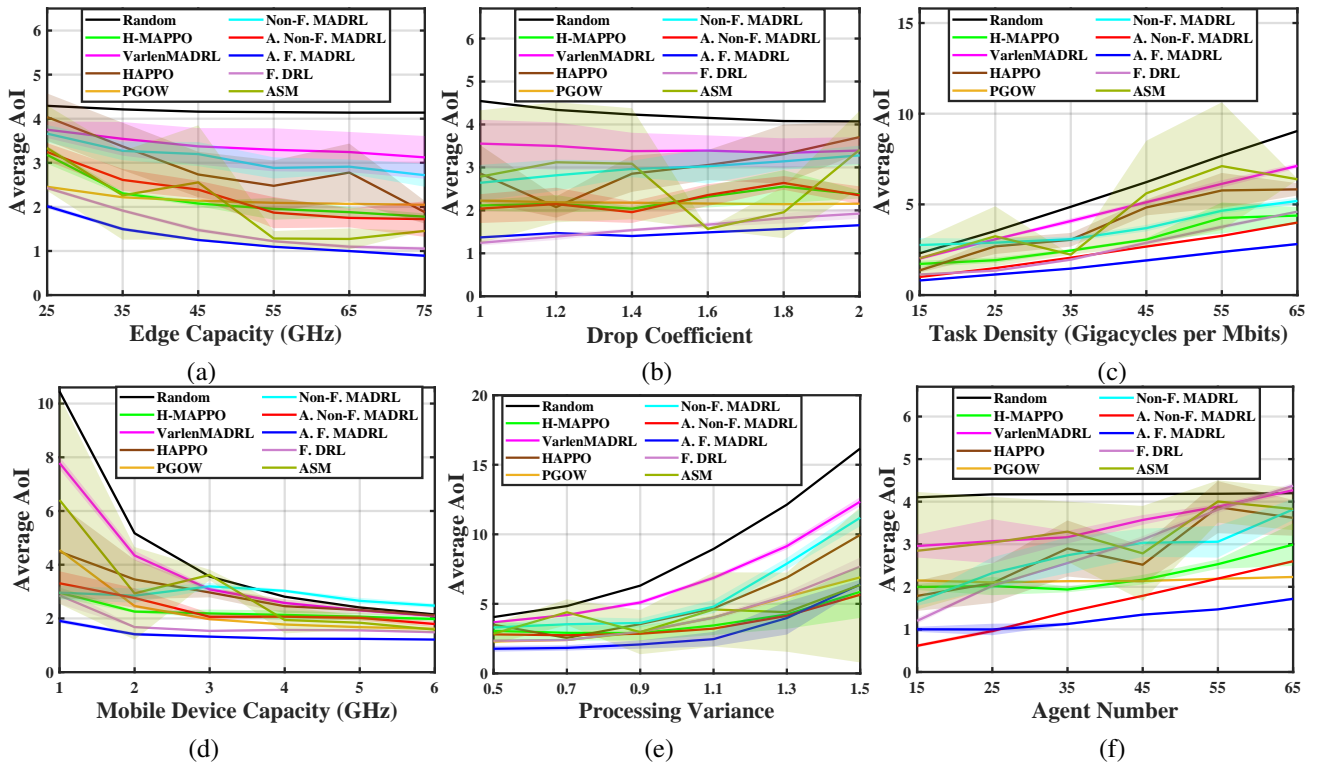


Fig. 5. Performance under different (a) processing capacities of edges, (b) drop coefficients, (c) task densities, (d) processing capacities of mobile devices, (e) processing variances, and (f) numbers of agents.

Gigacycles per Mbit), A. F. MADRL reduces the average AoI by up to 38.8% compared to F. DRL. These results demonstrate the effectiveness of our asynchronous trajectory collection mechanism, especially when computational resources are highly required.

**Mobile Capacity:** Fig. 5(d), presents results for different mobile device capacities. Our A. F. MADRL algorithm reduces average AoI by 20.4% on average compared to F. DRL algorithm. The performance differences diminish as mobile device computational capacities increase, primarily because devices with higher processing capabilities can handle most tasks locally. Consequently, the effectiveness of task scheduling diminishes.

**Processing Variance:** Fig. 5(e) demonstrates the performance of algorithms under different variances of processing time. In this particular experiment, processing times are modeled using a lognormal distribution. Our A. F. MADRL algorithm outperforms F. DRL algorithm by up to 30.7% when the processing variance is 1.1. These results demonstrate the robustness of our asynchronous trajectory collection mechanism under lognormal processing time distributions.

**Number of Mobile Devices:** Fig. 5(f) shows the performance with varying numbers of mobile devices and fixed edge servers. Specifically, under large-scale settings with 55 and 65 agents, where competition for edge-server queues becomes severe, A.F. MADRL achieves up to 61.4% and 60.7% performance improvements, respectively. These results demonstrate that our proposed framework scales robustly as competition for resources intensifies.

**Bandwidth of Time-Varying Channels:** We compare the

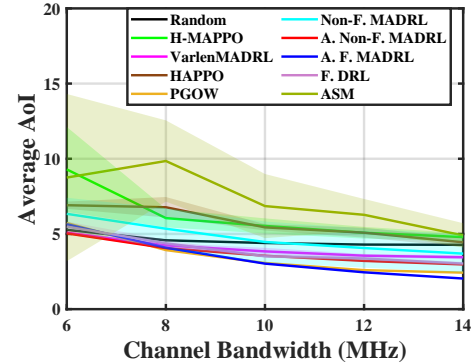


Fig. 6. Performance under different channel bandwidths with time-varying channels.

average AoI between proposed A.F. MADRL algorithm and other baselines in Section VII under different bandwidths. We set the channel parameters as in Table III, Appendix F. As in Fig. 6, traditional multi-agent DRL algorithms that train synchronously like MAPPO cannot converge well because the non-stationary time-varying channel causes additional asynchrony between agents. Our algorithm outperforms the best baseline F. DRL. by about 15.6 % on average. The performance gap between most algorithms narrow at lower channel bandwidth because as the transmitting time increases, the strategy of offloading to edges cannot work well compared to processing locally.

Additionally, we compare the computational requirement of our proposed A. F. MADRL algorithm and compare it with

TABLE I  
COMPUTATIONAL REQUIREMENTS OF DIFFERENT SCHEMES

A. F. MADRL	Non-F. MADRL	H-MAPPO	VarlenMARL
MFLOPs	17.86	16.39	10.90
			15.65

the other baseline algorithms: Non-F. MADRL, H-MAPPO, and VarlenMARL. These experiments were performed under identical system and network settings, including 20 agents, a batch size of 16, and the use of hybrid action spaces. The results are summarized in Table I.

As shown in Table I, the computational complexity of A. F. MADRL, measured in MFLOPs, is indeed higher than that of the baseline algorithms. However, it is important to note that our algorithm's complexity is only slightly higher than that of VarlenMARL ( $1.14\times$ ), which also employs the asynchronous decision-making mechanism as our algorithm. Crucially, the slightly increased computational cost of A. F. MADRL is accompanied by significant performance gains in terms of AoI reduction, as demonstrated in Fig. 5. We believe that this trade-off between computational cost and AoI performance is acceptable for many real-time applications where timely information updates are critical.

## VIII. CONCLUSION

In this paper, we proposed three schemes for computational task scheduling (including offloading and updating) age-minimal MEC in a semi-Markov game. First, we introduce a fractional RL framework for the single-agent scenario with fractional objectives. Second, we develop a fractional MARL framework for fractional scheme in multi-agent scenarios. We demonstrate that this framework theoretically converges to Nash equilibrium by showing that it is equivalent to an inexact Newton's method. Third, we present an asynchronous trajectory collection mechanism to address asynchronous multi-agent problems in the SMG. Evaluation results show significant performance improvements in average AoI for both the fractional framework and asynchronous trajectory collection mechanism.

In future work, it is worth concerning AoI-related challenges, such as timely multi-task remote inference [72], as well as problems that can be formulated with fractional objectives, including energy consumption and security satisfaction in MEC systems.

## REFERENCES

- [1] L. Jin, M. Tang, M. Zhang, and H. Wang, "Fractional deep reinforcement learning for age-minimal mobile edge computing," in *Proceedings of the AAAI Conference on Artificial Intelligence*, vol. 38, no. 11, 2024, pp. 12 947–12 955.
- [2] D. Katare, D. Perino, J. Nurmi, M. Warnier, M. Janssen, and A. Y. Ding, "A survey on approximate edge ai for energy efficient autonomous driving services," *IEEE Communications Surveys & Tutorials*, 2023.
- [3] Z. Xu, W. Jiang, J. Xu, Y. Deng, S. Cheng, and J. Zhao, "A power-grid-mapping edge computing structure for digital distributed distribution networks," *IEEE Transactions on Smart Grid*, 2023.
- [4] J. Jin, K. Yu, J. Kua, N. Zhang, Z. Pang, and Q.-L. Han, "Cloud-fog automation: Vision, enabling technologies, and future research directions," *IEEE Transactions on Industrial Informatics*, vol. 20, no. 2, pp. 1039–1054, 2023.
- [5] P. Porambage *et al.*, "Survey on multi-access edge computing for Internet of things realization," *IEEE Commun. Surveys & Tuts.*, vol. 20, no. 4, pp. 2961–2991, Jun. 2018.
- [6] Y. Mao, C. You, J. Zhang, K. Huang, and K. B. Letaief, "A survey on mobile edge computing: The communication perspective," *IEEE communications surveys & tutorials*, vol. 19, no. 4, pp. 2322–2358, 2017.
- [7] C. Zhu, G. Pastor, Y. Xiao, and A. Ylajaaski, "Vehicular fog computing for video crowdsourcing: Applications, feasibility, and challenges," *IEEE Communications Magazine*, vol. 56, no. 10, pp. 58–63, 2018.
- [8] X. Xu, K. Liu, K. Xiao, L. Feng, Z. Wu, and S. Guo, "Vehicular fog computing enabled real-time collision warning via trajectory calibration," *Mobile Networks and Applications*, vol. 25, pp. 2482–2494, 2020.
- [9] S. El Zaatar, M. Marei, W. Li, and Z. Usman, "Cobot programming for collaborative industrial tasks: An overview," *Robotics and Autonomous Systems*, vol. 116, pp. 162–180, 2019.
- [10] S. Kaul, R. Yates, and M. Gruteser, "Real-time status: How often should one update?" in *Proc. IEEE INFOCOM*, 2012, pp. 2731–2735.
- [11] S. Wang, Y. Guo, N. Zhang, P. Yang, A. Zhou, and X. Shen, "Delay-aware microservice coordination in mobile edge computing: A reinforcement learning approach," *IEEE Trans. Mobile Comput.*, vol. 20, no. 3, pp. 939 – 951, Mar. 2021.
- [12] M. Tang and V. W. Wong, "Deep reinforcement learning for task offloading in mobile edge computing systems," *IEEE Trans. Mobile Comput.*, vol. 21, no. 6, pp. 1985–1997, 2022.
- [13] R. D. Yates, Y. Sun, D. R. Brown, S. K. Kaul, E. Modiano, and S. Ulukus, "Age of information: An introduction and survey," *IEEE Journal on Selected Areas in Communications*, vol. 39, no. 5, pp. 1183–1210, 2021.
- [14] R. Talak and E. H. Modiano, "Age-delay tradeoffs in queueing systems," *IEEE Trans. Inform. Theory*, vol. 67, no. 3, pp. 1743–1758, 2021.
- [15] J. Hao, T. Yang, H. Tang, C. Bai, J. Liu, Z. Meng, P. Liu, and Z. Wang, "Exploration in deep reinforcement learning: From single-agent to multiagent domain," *IEEE Transactions on Neural Networks and Learning Systems*, 2023.
- [16] H. Ma, P. Huang, Z. Zhou, X. Zhang, and X. Chen, "Greenedge: Joint green energy scheduling and dynamic task offloading in multi-tier edge computing systems," *IEEE Transactions on Vehicular Technology*, vol. 71, no. 4, pp. 4322–4335, Apr. 2022.
- [17] N. Zhao, Z. Ye, Y. Pei, Y.-C. Liang, and D. Niyato, "Multi-agent deep reinforcement learning for task offloading in UAV-assisted mobile edge computing," *IEEE Trans. Wireless Commun.*, 2022.
- [18] X. He, S. Wang, X. Wang, S. Xu, and J. Ren, "Age-based scheduling for monitoring and control applications in mobile edge computing systems," in *Proc. IEEE INFOCOM*, May 2022.
- [19] X. Chen *et al.*, "Information freshness-aware task offloading in air-ground integrated edge computing systems," *IEEE J. Sel. Areas Commun.*, vol. 40, no. 1, pp. 243–258, Jan. 2022.
- [20] C. Xu *et al.*, "AoI-centric task scheduling for autonomous driving systems," in *Proc. IEEE INFOCOM*, May 2022.
- [21] R. Lowe, Y. I. Wu, A. Tamar, J. Harb, O. Pieter Abbeel, and I. Mordatch, "Multi-agent actor-critic for mixed cooperative-competitive environments," *Advances in neural information processing systems*, vol. 30, 2017.
- [22] T. Rashid, M. Samvelyan, C. S. De Witt, G. Farquhar, J. Foerster, and S. Whiteson, "Monotonic value function factorisation for deep multi-agent reinforcement learning," *The Journal of Machine Learning Research*, vol. 21, no. 1, pp. 7234–7284, 2020.
- [23] C. Yu, A. Veliu, E. Vinitsky, J. Gao, Y. Wang, A. Bayen, and Y. Wu, "The surprising effectiveness of ppo in cooperative multi-agent games," *Advances in Neural Information Processing Systems*, vol. 35, pp. 24 611–24 624, 2022.
- [24] W. Dinkelbach, "On nonlinear fractional programming," *Management science*, vol. 13, no. 7, pp. 492–498, May 1967.
- [25] J. Hu and M. P. Wellman, "Nash q-learning for general-sum stochastic games," *Journal of machine learning research*, vol. 4, no. Nov, pp. 1039–1069, 2003.
- [26] Y. Chen, J. Zhao, J. Hu, S. Wan, and J. Huang, "Distributed task offloading and resource purchasing in noma-enabled mobile edge computing: Hierarchical game theoretical approaches," *ACM Trans. Embed. Comput. Syst.*, vol. 23, no. 1, jan 2024.
- [27] H. Taka, F. He, and E. Oki, "Service placement and user assignment in multi-access edge computing with base-station failure," in *Proc. IEEE/ACM IWQoS*, Jun. 2022.
- [28] S. Liu, C. Zheng, Y. Huang, and T. Q. S. Quek, "Distributed reinforcement learning for privacy-preserving dynamic edge caching," *IEEE J. Sel. Areas Commun.*, vol. 40, no. 3, pp. 749–760, Mar. 2022.

[29] X. Wang, J. Ye, and J. C. Lui, "Decentralized task offloading in edge computing: A multi-user multi-armed bandit approach," in *Proc. IEEE Conference on Computer Communications (INFOCOM)*, May 2022.

[30] L. Huang, S. Bi, and Y.-J. A. Zhang, "Deep reinforcement learning for online computation offloading in wireless powered mobile-edge computing networks," *IEEE Trans. Mobile Comput.*, vol. 19, no. 11, pp. 2581 – 2593, Nov. 2020.

[31] S. Tuli *et al.*, "Dynamic scheduling for stochastic edge-cloud computing environments using A3C learning and residual recurrent neural networks," *IEEE Trans. Mobile Comput.*, vol. 21, no. 3, Mar. 2022.

[32] T. Liu *et al.*, "Deep reinforcement learning based approach for online service placement and computation resource allocation in edge computing," *IEEE Trans. Mobile Comput.*, 2022.

[33] Q. Li, X. Ma, A. Zhou, X. Luo, F. Yang, and S. Wang, "User-oriented edge node grouping in mobile edge computing," *IEEE Transactions on Mobile Computing*, 2021.

[34] Z. Feng, M. Huang, Y. Wu, D. Wu, J. Cao, I. Korovin, S. Gorbachev, and N. Gorbacheva, "Approximating nash equilibrium for anti-uav jamming markov game using a novel event-triggered multi-agent reinforcement learning," *Neural Networks*, vol. 161, pp. 330–342, 2023. [Online]. Available: <https://www.sciencedirect.com/science/article/pii/S0893608022005226>

[35] F. Yuan, S. Tang, and D. Liu, "Aoi-based transmission scheduling for cyber-physical systems over fading channel against eavesdropping," *IEEE Internet of Things Journal*, 2023.

[36] X. Fu, Q. Pan, and X. Huang, "Aoi-energy-aware collaborative data collection in uav-enabled wireless powered sensor networks," *IEEE Sensors Journal*, 2023.

[37] R. D. Yates, Y. Sun, D. R. Brown, S. K. Kaul, E. Modiano, and S. Ulukus, "Age of information: An introduction and survey," *IEEE J. Sel. Areas Commun.*, vol. 39, no. 5, pp. 1183–1210, 2021.

[38] F. Chiariotti, O. Vikhrova, B. Soret, and P. Popovski, "Peak age of information distribution for edge computing with wireless links," *IEEE Trans. Commun.*, vol. 69, no. 5, pp. 3176–3191, 2021.

[39] J. Zhu and J. Gong, "Optimizing peak age of information in mec systems: Computing preemption and non-preemption," *IEEE/ACM Transactions on Networking*, vol. 32, no. 4, pp. 3285–3300, 2024.

[40] —, "Multi-source peak age of information optimization in mobile edge computing systems," *IEEE Transactions on Networking*, 2025.

[41] E. T. Ceran, D. Gündüz, and A. György, "A reinforcement learning approach to age of information in multi-user networks with HARQ," *IEEE J. Sel. Areas Commun.*, vol. 39, no. 5, pp. 1412–1426, 2021.

[42] M. Akbari *et al.*, "Age of information aware vnf scheduling in industrial iot using deep reinforcement learning," *IEEE J. Sel. Areas Commun.*, vol. 39, no. 8, pp. 2487–2500, 2021.

[43] X. Chen *et al.*, "Age of information aware radio resource management in vehicular networks: A proactive deep reinforcement learning perspective," *IEEE Trans. Wireless Commun.*, vol. 19, no. 4, 2020.

[44] F. Wu, H. Zhang, J. Wu, Z. Han, H. V. Poor, and L. Song, "UAV-to-device underlay communications: Age of information minimization by multi-agent deep reinforcement learning," *IEEE Transactions on Communications*, vol. 69, no. 7, pp. 4461–4475, 2021.

[45] Z. Ren and B. Krogh, "Markov decision processes with fractional costs," *IEEE Transactions on Automatic Control*, vol. 50, no. 5, pp. 646–650, 2005.

[46] T. Tanaka, "A partially observable discrete time markov decision process with a fractional discounted reward," *Journal of Information and Optimization Sciences*, vol. 38, no. 1, pp. 21–37, 2017.

[47] W. Suttle, K. Zhang, Z. Yang, J. Liu, and D. Kraemer, "Reinforcement learning for cost-aware markov decision processes," in *Proceedings of the 38th International Conference on Machine Learning*, ser. Proceedings of Machine Learning Research, M. Meila and T. Zhang, Eds., vol. 139. PMLR, 18–24 Jul 2021, pp. 9989–9999. [Online]. Available: <https://proceedings.mlr.press/v139/suttle21a.html>

[48] Y. Xiao, W. Tan, and C. Amato, "Asynchronous actor-critic for multi-agent reinforcement learning," *Advances in Neural Information Processing Systems*, vol. 35, pp. 4385–4400, 2022.

[49] Y. Chen, H. Wu, Y. Liang, and G. Lai, "Varlenmarl: A framework of variable-length time-step multi-agent reinforcement learning for cooperative charging in sensor networks," in *2021 18th Annual IEEE International Conference on Sensing, Communication, and Networking (SECON)*. IEEE, 2021, pp. 1–9.

[50] J. Wang and L. Sun, "Reducing bus bunching with asynchronous multi-agent reinforcement learning," *arXiv preprint arXiv:2105.00376*, 2021.

[51] Y. Liang, H. Wu, and H. Wang, "Asm-ppo: Asynchronous and scalable multi-agent ppo for cooperative charging," in *Proceedings of the 21st International Conference on Autonomous Agents and Multiagent Systems*, 2022, pp. 798–806.

[52] —, "Asynchronous multi-agent reinforcement learning for collaborative partial charging in wireless rechargeable sensor networks," *IEEE Transactions on Mobile Computing*, 2023.

[53] Y. Sun, E. Uysal-Biyikoglu, R. D. Yates, C. E. Koksal, and N. B. Shroff, "Update or wait: How to keep your data fresh," *IEEE Trans. Inform. Theory*, vol. 63, no. 11, pp. 7492–7508, 2017.

[54] A. Arafa, R. D. Yates, and H. V. Poor, "Timely cloud computing: Preemption and waiting," in *Proc. Allerton*, 2019.

[55] Y. Sun and B. Cyr, "Sampling for data freshness optimization: Non-linear age functions," *Journal of Communications and Networks*, vol. 21, no. 3, pp. 204–219, 2019.

[56] A. Arafa, J. Yang, S. Ulukus, and H. V. Poor, "Age-minimal transmission for energy harvesting sensors with finite batteries: Online policies," *IEEE Transactions on Information Theory*, vol. 66, no. 1, pp. 534–556, 2019.

[57] M. Zhang, A. Arafa, J. Huang, and H. V. Poor, "Pricing fresh data," *IEEE J. Sel. Areas Commun.*, vol. 39, no. 5, pp. 1211–1225, 2021.

[58] Z. Tang, Z. Sun, N. Yang, and X. Zhou, "Age of information analysis of multi-user mobile edge computing systems," in *Proc. IEEE GLOBECOM*, Dec. 2021.

[59] J. Zhu and J. Gong, "Online scheduling of transmission and processing for aoi minimization with edge computing," in *Proc. IEEE INFOCOM WKSHPS*, May 2022.

[60] J. Li, Y. Zhou, and H. Chen, "Age of information for multicast transmission with fixed and random deadlines in IoT systems," *IEEE Internet of Things Journal*, vol. 7, no. 9, pp. 8178–8191, Sep. 2020.

[61] M. Ghavamzadeh, H. Kappen, M. Azar, and R. Munos, "Speedy q-learning," in *Proc. Neural Info. Process. Syst. (NIPS)*, vol. 24, 2011.

[62] L. Jin, M. Tang, J. Pan, M. Zhang, and H. Wang, "Asynchronous fractional multi-agent deep reinforcement learning for age-minimal mobile edge computing," 2024. [Online]. Available: <https://arxiv.org/abs/2409.16832>

[63] D. Adelman and A. J. Mersereau, "Relaxations of Weakly Coupled Stochastic Dynamic Programs," *Operations Research*, Jan. 2008, publisher: INFORMS. [Online]. Available: <https://pubsonline.informs.org/doi/abs/10.1287/opre.1070.0445>

[64] A. M. Fink, "Equilibrium in a stochastic  $n$ -person game," *Journal of science of the hiroshima university, series ai (mathematics)*, vol. 28, no. 1, pp. 89–93, 1964.

[65] P. Casgrain, B. Ning, and S. Jaimungal, "Deep q-learning for nash equilibria: Nash-dqn," *Applied Mathematical Finance*, vol. 29, no. 1, pp. 62–78, 2022.

[66] R. S. Dembo, S. C. Eisenstat, and T. Steihaug, "Inexact newton methods," *SIAM Journal on Numerical analysis*, vol. 19, no. 2, pp. 400–408, 1982.

[67] Y. C. Hu, M. Patel, D. Sabella, N. Sprecher, and V. Young, "Mobile edge computing—a key technology towards 5g," *ETSI white paper*, vol. 11, no. 11, pp. 1–16, 2015.

[68] J. Chung, C. Gulcehre, K. Cho, and Y. Bengio, "Empirical evaluation of gated recurrent neural networks on sequence modeling," *arXiv preprint arXiv:1412.3555*, 2014.

[69] J. G. Kubia, R. Chen, M. Wen, Y. Wen, F. Sun, J. Wang, and Y. Yang, "Trust region policy optimisation in multi-agent reinforcement learning," *arXiv preprint arXiv:2109.11251*, 2021.

[70] D. Monderer and L. S. Shapley, "Potential games," *Games and economic behavior*, vol. 14, no. 1, pp. 124–143, 1996.

[71] L. E. Blume, "The statistical mechanics of strategic interaction," *Games and economic behavior*, vol. 5, no. 3, pp. 387–424, 1993.

[72] M. K. C. Shisher, A. Piascenz, Y. Sun, and C. G. Brinton, "Computation and communication co-scheduling for timely multi-task inference at the wireless edge," *arXiv preprint arXiv:2501.04231*, 2025.

[73] V. Mnih *et al.*, "Human-level control through deep reinforcement learning," *Nature*, vol. 518, no. 7540, pp. 529–533, Feb. 2015.

[74] H. Van Hasselt, A. Guez, and D. Silver, "Deep reinforcement learning with double q-learning," in *Proceedings of the AAAI conference on artificial intelligence*, vol. 30, no. 1, 2016.

[75] Z. Wang, T. Schaul, M. Hessel, H. Hasselt, M. Lanctot, and N. Freitas, "Dueling network architectures for deep reinforcement learning," in *International conference on machine learning*. PMLR, 2016, pp. 1995–2003.

[76] M. Hausknecht and P. Stone, "Deep recurrent q-learning for partially observable mdps," in *2015 aaai fall symposium series*, 2015.

## APPENDIX A

## TIME COMPLEXITY OF INNER LOOP IN FQL ALGORITHM

**Proposition 1.** *The proposed FQL Algorithm satisfies the stopping condition  $\epsilon_i < -\alpha Q_i(\mathbf{s}_0, \mathbf{a}_i)$  for some  $\alpha \in (0, 1)$ , then after*

$$T_i = \left\lceil \frac{11.66 \log(2|\mathcal{Z}|/(E\zeta))}{\alpha^2} \right\rceil \quad (50)$$

steps of SQL in [61], the uniform approximation error  $\|Q_{\gamma_i}^* - Q_i\| \leq \epsilon_i$  holds for all  $i \in [E]$ , with a probability of  $1 - \zeta$  for any  $\zeta \in (0, 1)$ .

*Proof Sketch:* The main proof of Proposition 1 is based on [61]. Specifically, we can prove that the required  $T_i$  is proportional to  $Q_i^2/\epsilon_i^2$ , and hence corresponding to a constant upper bound.

Proposition 1 shows that the total steps needed  $T_i$  does not increase in  $i$ , even though the stopping condition  $\epsilon_i < -\alpha Q_i(\mathbf{s}_0, \mathbf{a}_i)$  is getting more restrictive as  $i$  increases.

APPENDIX B  
PROOF OF THEOREM 1

Define

$$\begin{aligned} \mathbf{a}^*(\gamma) &\triangleq \arg \max_{\mathbf{a} \in \mathcal{A}} (N_\gamma(\mathbf{s}_0, \mathbf{a}) - \gamma D_\gamma(\mathbf{s}_0, \mathbf{a})), \\ Q(\gamma) &\triangleq \max_{\mathbf{a} \in \mathcal{A}} (N_\gamma(\mathbf{s}_0, \mathbf{a}) - \gamma D_\gamma(\mathbf{s}_0, \mathbf{a})), \\ N(\gamma) &= N_\gamma(\mathbf{s}_0, \mathbf{a}^*(\gamma)) \text{ and } D(\gamma) = D_\gamma(\mathbf{s}_0, \mathbf{a}^*(\gamma)), \\ P(\gamma) &= \frac{N(\gamma)}{D(\gamma)}, \\ \mathbf{a}_i &\triangleq \arg \max_{\mathbf{a} \in \mathcal{A}} (N_k(\mathbf{s}_0, \mathbf{a}) - \gamma D_k(\mathbf{s}_0, \mathbf{a})), \end{aligned} \quad (51a)$$

for all  $\gamma \geq 0$ . In the remaining part of this proof, we use  $Q_i = Q_i(\mathbf{s}_0, \mathbf{a}_i)$ ,  $N_i = N_i(\mathbf{s}_0, \mathbf{a}_i)$ , and  $D_i = D_i(\mathbf{s}_0, \mathbf{a}_i)$  for presentation simplicity. Note that

$$\begin{aligned} &\frac{N(\gamma')}{D(\gamma')} - \frac{N_i}{D_i} \\ &\stackrel{(a)}{\geq} \frac{N(\gamma')}{D(\gamma')} - \frac{N(\gamma')}{D_i} - \gamma \left[ \frac{D(\gamma')}{D_i} - \frac{D(\gamma')}{D(\gamma)} \right] - \frac{\epsilon_i}{D_i} \\ &= [-Q(\gamma') + (\gamma_i - \gamma')D(\gamma')] \left( \frac{1}{D_i} - \frac{1}{D(\gamma')} \right) - \frac{\epsilon_i}{D_i}, \end{aligned}$$

where (a) is from the suboptimality of  $N_i$ . Sequences  $\{\gamma_i\}$ ,  $\{Q_i\}$ , and  $\{D_i\}$  generated by FQL Algorithm satisfy

$$\gamma_i - \gamma^* \geq \gamma_i - N_i/D_i = -Q_i/D_i > \epsilon_i/\alpha D_i, \quad (52)$$

for all  $i$  such that  $Q_i < 0$ . In addition, from the fact that  $N_i - \gamma_i D_i \leq N(\gamma^*) - \gamma_i D(\gamma^*)$  and  $N(\gamma^*) - \gamma^* D(\gamma^*) \leq N_i - \gamma^* D_i$  for all  $i \in [E]$ , it follows that  $(\gamma_i - \gamma^*)(D(\gamma^*) - D_i) \leq 0$ ,  $\forall i \in [E]$ , and hence  $\gamma_i \geq \gamma^*$  if and only if  $D_i \geq D(\gamma^*)$ . It follows from (52) that, for all  $i$ ,

$$\begin{aligned} \gamma_{i+1} - \gamma^* &= P_i - \gamma^* \leq (\gamma_i - \gamma^*) \left( 1 - \frac{D(\gamma^*)}{D_i} \right) + \frac{\epsilon_i}{D_i} \\ &\stackrel{(b)}{<} (\gamma_i - \gamma^*) \left( 1 + \alpha - \frac{D(\gamma^*)}{D_i} \right). \end{aligned}$$

Note that (b) is inducted from (52). Specifically, if  $\gamma_i < \gamma^*$ , then  $\gamma_{i+1} < \gamma^*$ . Therefore, we have that, if  $Q_i < 0$  then  $Q_{i+1} < 0$ , and hence that  $\epsilon_i \leq -\alpha Q_i$  for all  $i \in [E]$ . Let  $D_{\max} = \max_{\mathbf{s}, \mathbf{a}} \{ \frac{c_N(\mathbf{s}, \mathbf{a})}{c_D(\mathbf{s}, \mathbf{a})} \}$ ,  $D_{\min} = \min_{\mathbf{s}, \mathbf{a}} \{ \frac{c_N(\mathbf{s}, \mathbf{a})}{c_D(\mathbf{s}, \mathbf{a})} \}$ . We have  $\frac{D_{\min}}{D_{\max}} \in (0, 1)$ . Therefore, we can find an  $\alpha \in (0, \frac{D_{\min}}{D_{\max}})$ , such that  $(\gamma_{i+1} - \gamma^*)/(\gamma_i - \gamma^*) \in (0, 1)$  for all large enough  $i$ , which implies that  $\{\gamma_i\}$  converges linearly to  $\gamma^*$ .

APPENDIX C  
APPROXIMATING THE NASH OPERATOR

One can use the iterative best response algorithm to refine a joint action from an initial guess  $\mathbf{a}^{(0)}$  towards an approximate Nash operator. In each Q-learning iteration  $j$ , upon reaching a new state  $\mathbf{s}$ , each agent  $m$  sequentially updates its action to its best response, maximizing its individual Q-function given the other agents' actions from the previous iteration  $\mathbf{a}_{-m}^{(j-1)}$ . This best response  $\mathbf{a}_m^{(j)}$  for agent  $m$  is computed as:

$$\mathbf{a}_m^{(j)} = \arg \max_{\mathbf{a}_m} Q_{\gamma_m}^k(\mathbf{s}', \mathbf{a}_m, \mathbf{a}_{-m}^{(j-1)}), \quad (53)$$

where  $Q_{\gamma_m}^k$  denotes the Q-function of agent  $m$  at iteration  $j$ . The joint action is then updated to  $\mathbf{a}^{(j)} = (\mathbf{a}_1^{(j)}, \dots, \mathbf{a}_m^{(j)}, \dots, \mathbf{a}_M^{(j)})$ , incorporating the newly computed best response. After a few steps of this iterative refinement, the resulting joint action  $\mathbf{a}^{(j)}$  serves as our approximation of the Nash equilibrium in state  $\mathbf{s}'$ . Consequently, we can approximate  $\max_{\mathbf{a} \in \mathcal{A}} Q_{\gamma}^k(\mathbf{s}', \mathbf{a})$  with  $Q_{\gamma}^k(\mathbf{s}', \mathbf{a}^{(j)})$ , which is then used to update the Q-value in Equation (32). This iterative procedure allows agents to converge towards a Nash equilibrium by sequentially optimizing their actions in response to the actions of others, effectively approximating the action of the Nash operator.

APPENDIX D  
PROOF OF LEMMA 3

The Bellman equation form of  $V_{\gamma_m}$  of mobile device  $m$  is given by:

$$\begin{aligned} V_{\gamma_m}(\mathbf{s}, \boldsymbol{\pi}) &= \mathbb{E}_{\boldsymbol{\pi}} \{ c_{N_m}(\mathbf{s}, \mathbf{a}) - \gamma_m c_{D_m}(\mathbf{s}, \mathbf{a}) \\ &\quad + \delta \mathbb{E}_{Pr} [\delta V_{\gamma_m}(\mathbf{s}', \boldsymbol{\pi})] \}. \end{aligned}$$

Let  $\mathcal{B}(\mathcal{S})$  denote the Banach space of bounded real-valued functions on  $\mathcal{S}$  with the supremum norm. Let  $\mathbb{W}_{\boldsymbol{\pi}} : \mathcal{B}(\mathcal{S}) \rightarrow \mathcal{B}(\mathcal{S})$  be the mapping:

$$\begin{aligned} \mathbb{W}_{\boldsymbol{\pi}} V_{\gamma_m}(\mathbf{s}, \boldsymbol{\pi}) &= \min_{\boldsymbol{\pi}_m} \mathbb{E}_{\boldsymbol{\pi}} \{ [c_{N_m}(\mathbf{s}, \mathbf{a}) - \gamma_m c_{D_m}(\mathbf{s}, \mathbf{a}) \\ &\quad + \delta \mathbb{E}_{Pr} [V_{\gamma_m}(\mathbf{s}', \boldsymbol{\pi})]] \}. \end{aligned}$$

From [64], we have the following conclusion:

**Theorem C.3.** *(Contraction Mapping of  $\mathbb{W}_{\boldsymbol{\pi}}$ ) For any fixed  $\gamma_m$  and  $\mathbf{s} \in \mathcal{S}$ ,  $\mathbb{W}_{\boldsymbol{\pi}}$  is a contraction mapping of  $\mathbb{R}$ .*

By Theorem C.3, the sequence  $V_{\gamma_m}^0 = 0$ ,  $V_{\gamma_m}^{k+1} = \mathbb{W}_{\boldsymbol{\pi}} V_{\gamma_m}^k$  converges to the optimal cost  $V_{\gamma_m}^*(\mathbf{s})$ :

$$\begin{aligned} V_{\gamma_m}^*(\mathbf{s}) &= \min_{\boldsymbol{\pi}_m} \mathbb{E}_{\boldsymbol{\pi}} \{ c_{N_m}(\mathbf{s}, \mathbf{a}) - \gamma_m c_{D_m}(\mathbf{s}, \mathbf{a}) \\ &\quad + \delta \mathbb{E}_{Pr} [V_{\gamma_m}^*(\mathbf{s}')] \}. \end{aligned}$$

**Lemma C.5.**  $V_{\gamma_m}^*$  is continuous with respect to  $\gamma_m$ .

*Proof.* Define function  $f$  as

$$f(\gamma_m, \boldsymbol{\pi}, \mathbf{s}) = \mathbb{E}_{\boldsymbol{\pi}} \{ c_{N_m}(\mathbf{s}, \mathbf{a}) - \gamma_m c_{D_m}(\mathbf{s}, \mathbf{a}) + \delta \mathbb{E}_{P_r} [V_{\gamma_m}^*(\mathbf{s}')] \}.$$

From (54), we have

$$V_{\gamma_m}^*(\mathbf{s}) = \min_{\boldsymbol{\pi}_m} f(\gamma_m, \boldsymbol{\pi}, \mathbf{s}). \quad (54)$$

Since  $c_{N_m}(\mathbf{s}, \mathbf{a})$ ,  $c_{D_m}(\mathbf{s}, \mathbf{a})$  is continuous with respect to  $\boldsymbol{\pi}$ , we have  $f(\gamma_m, \boldsymbol{\pi}, \mathbf{s})$  is continuous with respect to  $\boldsymbol{\pi}$  and  $\gamma_m$ . Thus, as the set of  $\boldsymbol{\pi}$  is a compact set, by Berge's maximum theorem, we have  $V_{\gamma_m}^*(\mathbf{s})$  is continuous with respect to  $\gamma_m$ .  $\blacksquare$

Since  $c_{N_m}(\mathbf{s}, \mathbf{a})$ ,  $c_{D_m}(\mathbf{s}, \mathbf{a})$  are continuous with respect to  $\gamma_m$ , we have Nash operator  $\mathcal{N}_{\mathbf{a} \in \mathcal{A}}$  is continuous with respect to  $\gamma_m$ . From (34), we have  $\bar{N}_{\gamma_m}(\mathbf{s}), \bar{D}_{\gamma_m}(\mathbf{s})$  are continuous with respect to  $\gamma_m$ .

Define a compact and convex set  $\Gamma = [0, \bar{\gamma}]^M$ , where  $\bar{\gamma} = \max \left\{ \frac{c_{N,m}(\mathbf{s}, \mathbf{a})}{c_{D,m}(\mathbf{s}, \mathbf{a})} \right\}$ . We can thus define the mapping  $\mathbb{T} : \Gamma \rightarrow \Gamma$  of  $\gamma$  in Algorithm 2 as:

$$\mathbb{T}\gamma = \left[ \mathbb{E}_{\mathbf{s}_0 \sim \mu_0} \left[ \frac{\bar{N}_{\gamma_1}^*(\mathbf{s}_0)}{\bar{D}_{\gamma_1}^*(\mathbf{s}_0)} \right], \dots, \mathbb{E}_{\mathbf{s}_0 \sim \mu_0} \left[ \frac{\bar{N}_{\gamma_M}^*(\mathbf{s}_0)}{\bar{D}_{\gamma_M}^*(\mathbf{s}_0)} \right] \right]^T. \quad (55)$$

**Theorem C.4.** (Existence of Fixed Point) There exists a fixed point  $\gamma^*$  for mapping  $\mathbb{T} \in \Gamma$ , such that  $\mathbb{T}\gamma^* = \gamma^*$ .

*Proof.* Since  $\bar{D}_{\gamma_m}(\mathbf{s}_0) > 0$ , mapping  $\mathbb{T}$  is continuous on  $\gamma$ . We have  $\Gamma$  is a compact and convex set. By the Brouwer fixed point theorem, there exists a fixed point  $\gamma^* \in \Gamma$  for continuous mapping  $\mathbb{T}$ .  $\blacksquare$

Therefore, there exists  $\gamma^*$ , such that  $\mathbb{T}\gamma^* = \gamma^*$ . Then we have  $\mathbb{E}_{\mathbf{s}_0 \sim \mu_0} \left[ \frac{\bar{N}_{\gamma^*}(\mathbf{s}_0)}{\bar{D}_{\gamma^*}(\mathbf{s}_0)} \right] = \gamma^*$ . Thus, we have  $\mathbf{F}(\boldsymbol{\theta}^*, \gamma^*) = \mathbb{E}_{\mathbf{s}_0 \sim \mu_0} \left[ \bar{N}_{\gamma^*}^*(\mathbf{s}_0) \right] - \gamma^* \mathbb{E}_{\mathbf{s}_0 \sim \mu_0} \left[ \bar{D}_{\gamma^*}^*(\mathbf{s}_0) \right] = 0$ .

## APPENDIX E PROOF OF THEOREM 2

By Lemma 3, for each  $\gamma$ , there exists mapping  $\boldsymbol{\theta}(\gamma)$  that satisfies the NE conditions. For simplicity, we denote  $\boldsymbol{\theta}$  as  $\boldsymbol{\theta}(\gamma)$  and  $\boldsymbol{\theta}_i$  as  $\boldsymbol{\theta}(\gamma_i)$ . Assuming differentiability, these are the first-order necessary conditions where each agent optimizes its objective given the others' parameters:

$$\begin{aligned} W_m(\boldsymbol{\theta}, \gamma_m) &:= \nabla_{\boldsymbol{\theta}_m} F_m(\boldsymbol{\theta}, \gamma_m) \\ &= \nabla_{\boldsymbol{\theta}_m} N_m(\boldsymbol{\theta}) - \gamma_m \nabla_{\boldsymbol{\theta}_m} D_m(\boldsymbol{\theta}) = \mathbf{0} \end{aligned} \quad (56)$$

for all  $m \in \mathcal{M}$ . Let  $\mathbf{W}(\boldsymbol{\theta}, \gamma) = (W_1(\boldsymbol{\theta}, \gamma_1), \dots, W_M(\boldsymbol{\theta}, \gamma_M))$  be the stacked vector of these gradient conditions. The equilibrium condition is thus  $\mathbf{W}(\boldsymbol{\theta}, \gamma) = \mathbf{0}$ . We focus on a specific equilibrium point  $\boldsymbol{\theta}$  corresponding to  $\gamma$ . From Assumption 1, we have  $\mathbf{W}$  is invertible and  $\boldsymbol{\theta}$  is locally a differentiable function of

$\gamma$  around  $\gamma$ . By the Implicit Function Theorem (IFT), its Jacobian is given by:

$$\nabla_{\gamma} \boldsymbol{\theta}(\gamma) = -[\nabla_{\boldsymbol{\theta}} \mathbf{W}(\boldsymbol{\theta}, \gamma)]^{-1} [\nabla_{\gamma} \mathbf{W}(\boldsymbol{\theta}, \gamma)]. \quad (57)$$

We denote the Jacobian of  $\mathbf{W}$  with respect to  $\boldsymbol{\theta}$  as  $J_{\mathbf{W}}(\boldsymbol{\theta}, \gamma)$ . Its  $(m, n)$ -th block is given by:

$$\begin{aligned} (J_{\mathbf{W}}(\boldsymbol{\theta}, \gamma))_{mn} &= \nabla_{\boldsymbol{\theta}_n} W_m(\boldsymbol{\theta}, \gamma_m) = \nabla_{\boldsymbol{\theta}_n}^2 \theta_m F_m(\boldsymbol{\theta}, \gamma_m) \\ &= \nabla_{\boldsymbol{\theta}_n}^2 \theta_m N_m(\boldsymbol{\theta}) - \gamma_m \nabla_{\boldsymbol{\theta}_n}^2 \theta_m D_m(\boldsymbol{\theta}). \end{aligned} \quad (58)$$

We denote the Jacobian of  $\mathbf{W}$  with respect to  $\gamma$  as  $\nabla_{\gamma} \mathbf{W}$ . Its  $(m, n)$ -th block is given by

$$\begin{aligned} &\frac{\partial W_m}{\partial \gamma_n}(\boldsymbol{\theta}, \gamma) \\ &= \frac{\partial}{\partial \gamma_n} [\nabla_{\boldsymbol{\theta}_m} N_m(\boldsymbol{\theta}) - \gamma_m \nabla_{\boldsymbol{\theta}_m} D_m(\boldsymbol{\theta})] \\ &= -\delta_{mn} \nabla_{\boldsymbol{\theta}_m} D_m(\boldsymbol{\theta}) \end{aligned} \quad (59)$$

The  $n$ -th column of  $\nabla_{\gamma} \mathbf{W}$ , denoted  $\frac{\partial W}{\partial \gamma_n}(\boldsymbol{\theta}, \gamma)$ , is given by:

$$\frac{\partial W}{\partial \gamma_n}(\boldsymbol{\theta}, \gamma) = \begin{pmatrix} \mathbf{0} \\ \vdots \\ \mathbf{0} \\ -\nabla_{\boldsymbol{\theta}_n} D_n(\boldsymbol{\theta}) \\ \mathbf{0} \\ \vdots \\ \mathbf{0} \end{pmatrix}. \quad (60)$$

Let  $((J_{\mathbf{W}})^{-1})_{mk}$  denote the  $(m, k)$ -th block of the inverse matrix  $(J_{\mathbf{W}})^{-1}$ . By the IFT formula, the  $j$ -th block of the sensitivity vector is given by:

$$\begin{aligned} \frac{\partial \boldsymbol{\theta}_m}{\partial \gamma_n} &= -\sum_{k=1}^M ((J_{\mathbf{W}}(\boldsymbol{\theta}, \gamma))^{-1})_{mk} \left( \frac{\partial W_k}{\partial \gamma_n}(\boldsymbol{\theta}, \gamma) \right) \\ &= ((J_{\mathbf{W}}(\boldsymbol{\theta}, \gamma))^{-1})_{mn} \nabla_{\boldsymbol{\theta}_n} D_n(\boldsymbol{\theta}). \end{aligned} \quad (61)$$

We then have the bound as follows.

**Lemma C.6.** By Assumption 3 and 1, there exists  $\kappa \in (0, 1)$ ,  $J_{\mathbf{W}}$  is invertible, and the block  $L_{\infty}$  norm of its inverse is bounded by:

$$\| (J_{\mathbf{W}})^{-1} \|_{\infty} \leq \frac{\max_k \| ((J_{\mathbf{W}})_{kk})^{-1} \|}{1 - \kappa}.$$

*Proof.* From Assumption 3 and 1, we have that

$$\begin{aligned} &\sum_{l \neq k} \| ((J_{\mathbf{W}})^{-1})_{kk} \|^2 \| ((J_{\mathbf{W}})^{-1})_{kl} \| \\ &\leq \| ((J_{\mathbf{W}})^{-1})_{kk} \|^2 \| ((J_{\mathbf{W}})^{-1})_{kl} \| \\ &\leq \frac{KH_{\text{int}}}{\mu} < 1. \end{aligned} \quad (62)$$

Thus, there exists  $\kappa \in (0, 1)$ , such that

$$\kappa = \frac{KH_{\text{int}}}{\mu}.$$

The block inverse formula gives

$$\begin{aligned} & ((J_W)^{-1})_{kn} \\ &= \delta_{kn}((J_W)_{kk})^{-1} - \sum_{l \neq k} ((J_W)_{kk})^{-1} (J_W)_{kl} ((J_W)^{-1})_{ln}. \end{aligned} \quad (63)$$

Taking the norm and summing over  $n$ ,

$$\begin{aligned} & \sum_n \|((J_W)^{-1})_{kn}\| \\ & \leq \|((J_W)_{kk})^{-1}\| + \sum_{l \neq k} \|((J_W)_{kk})^{-1} (J_W)_{kl}\| \\ & \quad \cdot \sum_n \|((J_W)^{-1})_{ln}\|. \end{aligned} \quad (64)$$

Taking  $\max_k$  on both sides,

$$\begin{aligned} & \max_k \sum_n \|((J_W)^{-1})_{kn}\| \\ & \leq \max_k \|((J_W)_{kk})^{-1}\| + \kappa \max_k \sum_n \|((J_W)^{-1})_{kn}\|. \end{aligned} \quad (65)$$

Thus, we have

$$(1 - \kappa) \max_k \sum_n \|((J_W)^{-1})_{kn}\| \leq \max_k \|((J_W)_{kk})^{-1}\|,$$

and

$$\max_k \sum_n \|((J_W)^{-1})_{kn}\| \leq \frac{\max_k \|((J_W)_{kk})^{-1}\|}{1 - \kappa}. \quad \blacksquare$$

Using Lemma C.6 and Assumption 1, there exists  $\kappa \in (0, 1)$ , such that

$$\|((J_W)^{-1})\|_{\infty} \leq \frac{1}{\mu(1 - \kappa)}. \quad (66)$$

We can solve for the residual  $r_i$  as:

$$\begin{aligned} r_i &= \mathbf{F}(\boldsymbol{\theta}_i, \gamma_i) + J_{\mathbf{F}}(\boldsymbol{\theta}_i, \gamma_i) s_i \\ &= [I - J_{\mathbf{F}}(\boldsymbol{\theta}_i, \gamma_i) J_{\mathbf{F}}'(\boldsymbol{\theta}_i, \gamma_i)^{-1}] F(\boldsymbol{\theta}_i, \gamma_i). \end{aligned} \quad (67)$$

The Inexact Newton method requires the residual to satisfy  $\|r_i\| \leq \eta_i \|\mathbf{F}(\boldsymbol{\theta}_i, \gamma_i)\|$  for some forcing sequence  $\{\eta_i\}$ . From (67), (66) and Assumption 2, 3, we have that

$$\begin{aligned} & \eta_i \\ &= \|I - J_{\mathbf{F}}(\boldsymbol{\theta}_i, \gamma_i) J_{\mathbf{F}}'(\boldsymbol{\theta}_i, \gamma_i)^{-1}\|_{\infty} \\ &\leq \max_m \sum_{n \neq m} \frac{1}{|D_n(\boldsymbol{\theta}_i)|} \sum_{k \in \mathcal{N}_m^{grad}} \|\nabla_{\boldsymbol{\theta}_{k,i}} F_m(\boldsymbol{\theta}_i, \gamma_{m,i})\|_{\infty} \\ &\quad \cdot \|((J_W(\boldsymbol{\theta}_i, \gamma_i)^{-1})_{kn}\|_{\infty} \cdot \|\nabla_{\boldsymbol{\theta}_n} D_n(\boldsymbol{\theta}_i)\|_{\infty} \\ &\leq \max_m \frac{C_D C_{int}}{D_{min}} \sum_{k \in \mathcal{N}_m^{grad}} \left( \sum_{n \neq m} \|((J_W(\boldsymbol{\theta}_i, \gamma_i)^{-1})_{kn}\|_{\infty} \right) \\ &\leq \frac{K C_D C_{int}}{\mu D_{min}(1 - \kappa)} = \frac{C_D C_{int}}{D_{min}(1/K - H_{int})}. \end{aligned} \quad (68)$$

Thus, there exists  $\eta_{max} = \frac{C_D C_{int}}{D_{min}(1/K - H_{int})} < 1$  such that  $\eta_i \leq \eta_{max}$ .

Therefore, under the stated assumptions, there exists a neighborhood  $\mathcal{U}' \subseteq \mathcal{U}(\gamma^*)$  such that if  $\gamma^0 \in \mathcal{U}'$ , the sequence  $\{\gamma_i\}$  converges to  $\gamma^*$ . The outer-loop iteration in Algorithm 2 converges to NE of game  $\mathbf{G}$  linearly.

## APPENDIX F ASYNCHRONOUS FRACTIONAL MULTI-AGENT DRL NETWORKS

As shown in Fig. 7, for each mobile device, our algorithm contains R-D3QN and R-PPO networks for discrete and continuous action space as well as interactions between agents and history information.

### A. R-D3QN Module

D3QN is a modified version of deep Q-learning [73] equipped with double DQN technique with target Q to overcome overestimation [74] and dueling DQN technique which separately estimates value function and advantage function [75]. And our R-D3QN structure is inspired by DRQN [76] which allows networks to retain context and memory from history events and environment states. The key idea is to learn a mapping from states in state space  $S^O$  to the Q-value of actions in action space  $A^O$ . When the policy is learned and updated to the mobile device, it can selective offloading actions with the maximum Q-value to maximize the expected long-term reward. Apart from traditional deep Q-learning, it has a target Q-function network to compute the expected long-term reward based on the optimal action chosen with the traditional Q-function network to solve the overestimation problem. What's more, both the Q-function networks contain the advantage layer and value layer, which are used to estimate the value of the state and the relative advantage of the action. What's more, we take advantage of a GRU module to provide history information of other agents' decisions and environment states.

### B. R-PPO Module

R-PPO mainly includes two networks: policy network and value network. Policy network is responsible for producing actions based on networks. It outputs mean and standard deviation vectors for continuous action and probability distribution for discrete network. The value network computes the advantage values and estimates the expected return of the current state. Similar to R-D3QN network, it has an additional GRU module to memorize the state-action pairs from history and other agents to enhance the information contained by the state based on which the value network estimates the state value.

## APPENDIX G EXPERIMENTAL SETUP AND HYPERPARAMETERS

To ensure the reproducibility of our reported results, this appendix provides a comprehensive list of the environment settings, communication model parameters, algorithmic hyperparameters, and training details used in our simulations.

### A. Environment and Task Parameters

The default parameters for the Mobile Edge Computing (MEC) environment and the computational tasks are detailed in Table II. These settings were used for all experiments unless explicitly varied, as noted in the main text.

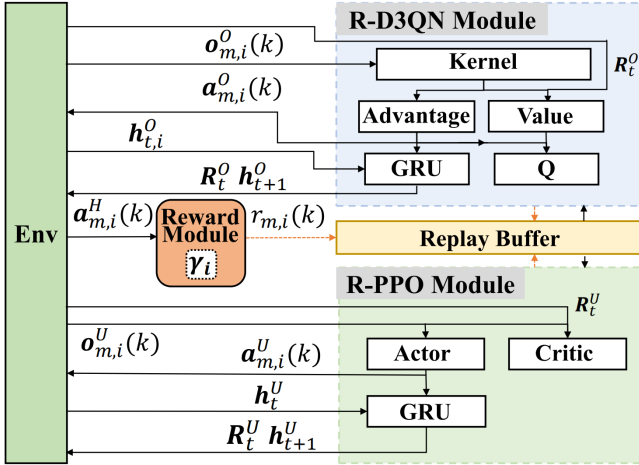


Fig. 7. Illustration on the proposed fractional multi-agent DRL framework of D3QN and PPO module with RNN networks including reward module with proposed fractional scheme and GRU module with asynchronous trajectory collection mechanism.

TABLE II  
DEFAULT ENVIRONMENT AND TASK PARAMETER SETTINGS

Parameter	Value
Number of mobile devices	20
Number of edge nodes	2
Capacity of mobile devices	2.5 GHz
Capacity of edge nodes	41.8 GHz
Task size	30 Mbits
Task density	0.297 gigacycles per Mbits
Drop coefficient ( $\bar{Y}$ )	1.5

### B. Communication Model Parameters

The general parameters for the wireless communication model, as described in Equation (1), are listed below.

- Transmit power ( $p_m$ ): 20 dBm
- Background noise power ( $\eta_0$ ): -114 dBm
- Path loss exponent ( $\alpha$ ): 3

For the specific experiment involving time-varying channels (Figure 6), the parameters were set according to Table III.

TABLE III  
CHANNEL PARAMETER SETTINGS FOR TIME-VARYING EXPERIMENTS  
(FIG. 6)

Parameter	Value
Number of mobile devices	10
Transmit power	20 dBm
Background noise power	-114 dBm
Path loss exponent	3

### C. Algorithmic Hyperparameters for A.F. MADRL

The performance of our proposed Asynchronous Fractional Multi-Agent DRL (A.F. MADRL) algorithm depends on a set of key hyperparameters. Table IV provides the specific values used for our implementation, which are essential for replicating our learning-based results.

TABLE IV  
HYPERPARAMETERS FOR THE A.F. MADRL ALGORITHM

Category	Hyperparameter	Value
General RL	Discount Factor ( $\delta$ )	0.99
	Replay Buffer Size	100,000
	Batch Size	64
	Target Network Update Rate ( $\tau$ )	0.005 (soft update)
R-D3QN (Offloading)	Learning Rate	1e-4 (Adam Optimizer)
	$\epsilon$ -Greedy Schedule	Linear decay from 1.0 to 0.05 over 500 episodes
R-PPO (Updating)	Actor Learning Rate	3e-4 (Adam Optimizer)
	Critic Learning Rate	1e-3 (Adam Optimizer)
	PPO Clipping Parameter ( $\epsilon$ )	0.2
	Entropy Coefficient	0.01
Network Architecture	GRU Hidden Units	128
	Fully Connected Layers (Post-GRU)	Two layers with [256, 128] units and ReLU activation
Fractional Module	$\gamma$ Update Frequency	Every 50 episodes

### D. Training Details

All algorithms were implemented using PyTorch. The training was conducted on a server equipped with an AMD EPYC 7763 CPU and an NVIDIA RTX 4090 GPU. To ensure the stability and reliability of our results, we used fixed random seeds for network initialization and environment generation. Each experiment was run for 1000 episodes (or 1500 if convergence was slower), and the final reported results are the average of five independent runs, with the shaded areas in plots representing the standard deviation across these runs.